STUDY OF THE BEHAVIOUR OF MULTI-METALLIC SYSTEMS UNDER HIGH-VELOCITY IMPACT LOADS

KMSR Wijekoon

(228072F)

Degree of Master of Science

Department of Civil Engineering

Faculty of Engineering

University of Moratuwa
Sri Lanka

October 2023

STUDY OF THE BEHAVIOUR OF MULTI-METALLIC SYSTEMS UNDER HIGH-VELOCITY IMPACT LOADS

KMSR Wijekoon

228072F

Thesis/Dissertation submitted in partial fulfillment of the requirements for the degree
Degree of Master of Science

Department of Civil Engineering
Faculty of Engineering

University of Moratuwa
Sri Lanka

October 2023

Declaration of the Candidate and Supervisor

"I declare that this is my work and this thesis does not incorporate without acknowledgment any material previously submitted for a Degree or Diploma in any other University or institute of higher learning and to the best of my knowledge and belief it does not contain any material previously published or written by an person except where the acknowledgment is made in the text.

Also, I hereby grant to the University of Moratuwa the non-exclusive right reproduce and distribute my thesis, in whole or in part in print, electronic or other medium. I retain the right to use this content in whole or part in the future.

Signature: Date: 15/09/2023

The above candidate has carried out research for the Master's thesis under my supervision.

Name of the supervisor: Dr. Lakshitha Fernando

Signature of the supervisor: Date: 26/01/2024

Acknowledgments

First and foremost, I would like to express my sincere gratitude to my research supervisor, Dr. Lakshitha Fernando, for providing me the opportunity to do research under his invaluable guidance throughout. Without his support, this would have not been possible.

I would like to say my special thanks to Dr. Hasitha Damruwan for the valuable comments during the progress reviews which inspired me to think out of the box.

In addition, I would like to acknowledge all academic staff members of the Department of Civil Engineering, for their constant support throughout.

I would like to show my gratitude for the financial assistance provided by the Structural Engineering Division, University of Moratuwa.

Finally, and most importantly, I am thankful to my family and friends for their constant source of inspiration and moral support.

Abstract

The behavior of multi-material layered systems under high-velocity impact loads, such as impact and blast scenarios, has gained significant attention from researchers over the past years due to its extensive applications in the automobile and aerospace industries, and ballistic armor and blast resilient structures. The focus is being shifted to multi-material systems over monolithic systems due to their superior characteristics in stress attenuation and energy absorption, and high preference for lightweight structures.

In this research, an attempt has been made to investigate the impact-induced stress wave propagation through a multi-metallic layered system that is subjected to high-velocity impact loads. This study consists of two major components. 1) Elastic wave propagation and 2) Shock wave propagation. For the elastic wave propagation, four different test cases including a steel monolithic target, steel-titanium and steel-aluminium bi-metallic targets, and a steel-titanium-aluminium tri-metallic target, were considered. They were subjected to a low-velocity (180 ms^{-1}) impact where only elastic waves are anticipated to be generated in the target. For shock wave propagation, only a steel monolithic target was considered which was subjected to an impact velocity of 350 ms^{-1}. For both cases, numerical and analytical frameworks were developed to simulate the material response. The LS-DYNA finite element package was used to develop two-dimensional axisymmetric numerical models, and it was validated against the existing experimental results obtained from a single-stage gas gun test which were in good agreement.

The analytical models which were the main focus of the present research were implemented in MATLAB which monitors and resolves the interaction of each propagation wave and then provides the overall response of the flyer-target system. The analytical model was validated against the results obtained from the validated numerical models considering stress-time histories.

The outputs acquired from the analytical model for elastic wave propagation agree with that of the numerical model with reasonable accuracy. However, the developed analytical model for shock wave propagation gives reasonable results only up to the separation of the flyer and multi-material target where a significant variation can be identified between results after the separation. The developed models can be used to

find the most optimum configuration in terms of stress attenuation for a given set of metallic materials which reduces the time and cost associated with high-velocity impact tests. Also, they can be used to find the required bonding strength to avoid debonding at material interfaces that cannot be obtained from experiments.

Keywords: elastic waves, shock waves, multi-metallic, numerical modeling, wave interaction, analytical modeling

Table of Contents

List of Tables

List of Figures

List of Abbreviations

Abbreviation	Description
EOS	Equation Of State
HEL	Hugoniot Elastic Limit
FEM	Finite Element Modeling
SPH	Smooth Particle Hydrodynamics
PDV	Photonic Doppler Velocimetry
CFRP	Carbon Fibre Reinforced Polymer

List of Symbols

Symbol	Description
σ_H	Hydrostatic stress
$\sigma_{11}, \sigma_{22}, \sigma_{33}$	Principal stresses
$\sigma_{12}, \sigma_{21}, \sigma_{13}, \sigma_{31}, \sigma_{23}, \sigma_{32}$	Inplane shear stresses
A	Yield stress
B	Strain hardening constant
n	Strain hardening coefficient
C*	Strengthening coefficient of strain rate
m	Thermal softening coefficient
T	Temperature in Kelvin degrees
σ	Stress
ε	Strain
C_B	Bulk sound speed
S1	Hugoniot slope coefficient
S2, S3	Higher order Hugoniot slope coefficients
υ	Poisson's ratio
Y_d	Dynamic yield strength
ρ	Mass density
V	Particle velocity
U	Shock velocity
e	Specific internal energy
E	Young's modulus
C	Elastic wave velocity

1 INTRODUCTION

1.1 Overview

Due to the immense usage of multi-material systems in the automobile and aerospace industries, and ballistic armor and blast resilient structures, researchers are struggling to develop more effective and optimized systems to mitigate the adverse effects of intentional and accidental extreme loads [1]. Also, enhancing the safeguarding of existing and future infrastructures, especially in military-related structures has become a major concern for the modern structural engineer as those structures are usually subjected to impact and explosive loads generated due to vehicle and/or aircraft crashes, bombing, and accidental and intentional explosions [2].

Multi-material systems have been found more efficient over monolithic targets due to their inherent characteristics such as enhanced stress attenuation and robustness, and weight reduction. As a result, distinct multi-material forms ranging from non-metallic materials to metallic alloys including foams, polymers, and ceramics have been taken into account in previous studies. A careful arrangement of various materials has been employed to achieve the desired properties in functionally graded multi-material systems [3].

Broadly stress waves can be divided into two categories: elastic waves and shock waves. When a stress wave's magnitude is greater than the material's HEL (Hugoniot Elastic Limit) value, there would be a shock wave along with a foregoing elastic wave. Otherwise, there would be only an elastic wave. Usually, when the developed strain rates are in the region 10^2 - 10^4/s, high-pressure dynamic loads are generated inside the material, causing elastic wave propagation through metallic materials. When it exceeds 10^4/s, there will be shock waves [4].

The conventional stress-strain curve which is for static loads does not represent the relationship between stress and strain at high strain rates. The associated material properties with those conventional curves such as elastic modulus, yield strength, ultimate strength, and elongation are inappropriate to characterize the dynamic behavior of materials [5]. Therefore, representative stress-strain curves have been developed to simulate the behavior of materials during high strain rates considering

that there are no lateral strains and deformation is limited to one dimension.

A uniaxial strain state arises during high strain rate phenomena where the material is not given enough time to deform laterally. Later on, stresses will diminish and a state that is close to uniaxial stress may arise as relief waves from the lateral surfaces arrive and lateral deformations start to occur [5].

Numerous studies have been conducted on stress wave propagation in multi-material systems for decades which resulted in advanced numerical models and analytical frameworks that are capable of simulating the complex behavior of multi-metallic systems under high-velocity impact loads. However, those developed models consist of some drawbacks which limit their applicability in real-world applications.

The present study consists of two major components. 1) Elastic wave propagation and 2) Shock wave propagation. Numerical models and analytical models were developed for both cases separately.

1.2 Importance of having a realistic analytical and/ or numerical model

Exploring the behavior of multi-metallic targets under extreme loads by only conducting trial and error physical tests consists of some major drawbacks such as associated cost and time.

Further, to characterize the deficiencies involved with multi-metal targets such as debonding at interfaces and spalling failures, it would be beneficial to have an alternative method other than physical testing because of the extremely fast nature of the impact.

Also, the required bonding strength to avoid any debonding at the interfaces is one of the crucial outputs of this study. However, it is almost impossible to get it through a physical test and can be only obtained by an analytical or numerical model.

The effectiveness of multi-material systems in attenuating stress waves varies with the arrangement of materials and to identify the most effective order for a given set of materials, the same test should be repeated for each test case that is not economically feasible. So, it is necessary to have a realistic analytical or numerical model to simulate the complex behavior of metallic targets at high strain rates.

1.3 Problem Statement

Even though several analytical and numerical models have been developed to simulate the propagation of stress waves within a multi-material system in previous studies, they are only applicable to some specified cases (not generalized models). Most of the analytical models are based on assumptions that are far away from the real applications and therefore they are only applicable to specified hypothetical cases.

Chen and Chandra [6] developed an analytical solution to study wave propagation with high amplitudes within layered heterogeneous material systems, which is restricted only to periodic laminates and, semi-infinite impactors and targets. Composite materials have been idealized to periodical laminates due to the difficulties met in characterizing engineering composites. Also, in some research, homogenization techniques have been incorporated to simplify the analysis of shock wave propagation. Vinamra and Bhattacharya [7] idealized that the materials are elastically homogenous (same yield strength, Young's modulus, and density) and only heterogenous for shock waves. In that model, transmission as well as reflection of elastic waves at material interfaces are not accounted which is not realistic.

Gazons et al. [8] derived the exact solutions for the stress and velocity time histories of plate impact tests. However, it is applicable only for Goupillaud type (each layer consists of equal wave travel time) multi-material targets. Also, in some already developed models, the separation of target materials and flyer is not allowed even though tensile stresses are generated at the interfaces. To study how a layered, heterogeneous system responds to a one-dimensional effect, Satyendra and Singh [1] developed a more realistic analytical model. This is a generalized model that can be used for finite non-periodic, non-Goupillaud flyer and target systems. However, the separation of target materials is not allowed which cannot be used to obtain the required bonding strength to avoid debonding, the time of separation, and the response of target materials after the separation.

As discussed above, the existing analytical models do not work for arbitrary multi-material systems and only work for some specified cases. Also, the existing numerical models are not efficient in terms of required computational power while some Lagrangian-based numerical models result in excessive mesh deformations

under extreme loads. So, the primary objective of this study is to come up with a realistic analytical and numerical model that is applicable to any given case.

1.4 Scope of the Study

The present work on multi-metallic targets is limited to the prediction of material response under high-velocity impacts where the impactor travels along the direction of the axis of the target (uniaxial). The developed models are not capable of predicting the material behavior under oblique impacts. Further, these studies are confined to flyers and target materials with the same diameter. Also, for the elastic wave propagation study, both monolithic and multi-metallic targets were considered while for the shock wave propagation study, only monolithic targets were considered.

1.5 Aim and Objectives

While the broad aim of this research is focused on developing a numerical model and an analytical model for predicting stress wave propagation through multi-metallic systems under high-velocity impacts, the following specific objectives were addressed.

- Identify the shortcomings and limitations of existing analytical and numerical models when applying to multi-metallic systems.
- Develop realistic analytical and numerical models to simulate the elastic wave propagation and shock wave propagation through multi-metallic systems and validate the models using experimental results available in the literature.

1.6 Methodology

Initially, a thorough literature review was carried out on stress wave propagation theories, governing equations for stress wave interactions, constitutive material models to simulate the behavior of metals at high strain rates, and numerical modeling techniques.

The limitations and shortcomings of the existing analytical and numerical models were identified. As the first step, a realistic analytical and numerical model was

developed to simulate the elastic wave propagation. By idealizing the 3D model into a 2D axisymmetric model, a computationally efficient numerical model was developed in the LS-DYNA finite element package.

The developed numerical model was validated by comparing its output with the experimentally obtained free surface velocity profiles. Then an analytical model was implemented in MATLAB to track each wave propagation and solve the corresponding wave interactions. The analytical model was validated by comparing stress-time histories with the outputs obtained from the already validated numerical model. Eventually, the numerical and analytical models that were developed were extended to simulate shock wave propagation in multi-metallic systems.

1.7 Chapter Organisation

This research thesis consists of 6 Chapters. Following the present introductory Chapter, Chapter 2 begins with a literature review, explaining state of the art of protective mechanisms against impact loads, numerical modeling techniques, and analytical frameworks carried out in previous studies to simulate the response of multi-material systems under high-velocity impact loads.

Chapter 3 describes the method followed to develop the 2D axisymmetric numerical model in LS-DYNA. Initially, it describes the incorporated constitutive material model along with the Equation of State (EOS). Following that, the idealization of the 3D model into a 2D axisymmetric model is present. Then, the imposed boundary conditions and keywords used to define the interaction between the flyer and the target are explained. Finally, to validate, the developed numerical models were compared against the experimentally obtained free surface history profiles for both elastic and shock waves is given.

Chapter 4 includes a comprehensive study of the fundamental theories that govern the stress wave propagation in a material. Following that, the governing equations for both elastic and shock wave propagation have been derived. It concludes with the validation of the developed analytical models compared against the stress–time variations obtained from numerical models. Chapter 5 concludes the research thesis with important findings of the study and necessary recommendations for future works.

2 LITERATURE REVIEW

This chapter reviews the state of the art of protective mechanisms against impact loads and the latest literature on recent developments in analytical and numerical approaches to simulate high-velocity impact events and their limitations.

2.1 Protective mechanisms against impact loads – State of the Art

The safeguarding of civil and military-related structures was an area of major concern for structural engineers over the 20th century. The catastrophic failures of structures caused by the extreme loads such as impact and blast generated due to bombing, explosions, and aircraft crashes during World War I and II motivated the researchers to inspire more efficient protective mechanisms [9]. As a result, a variety of impact and blast-resistant mechanisms have been developed over the years. In the 1970s, nuclear power plants became popular in developed countries as the most efficient energy generation method. However, with the growth of intentional terrorist attacks, the safety of containment vessels in nuclear power plants became a major concern due to their potential to explode [2]. Meantime, in the automotive and aerospace industries, engineers struggled to develop vehicles with advanced crashworthiness characteristics. Employing impact resistance mechanisms in vehicles was found to be more effective in those cases. Likewise, the interest of the researchers was shifted towards introducing innovative protective mechanisms against impact loads because of its immense usage in a variety of industries.

The magnitude of the load generated during a high-velocity impact varies with the impactor characteristics such as size and shape, hardness or rigidity, and impact velocity and direction. Therefore, it has become more difficult to come up with efficient protective mechanisms for a given application [10]. In previous attempts, two major approaches to improve the structures' impact resistance can be identified. The former is to improve the impact resistance capacities of materials while the latter is to implement protective mechanisms against the impact loads ahead of the structures [11].

The ability of a material to absorb and dissipate energy during impact loads is known as impact resistance [12]. Multi-material layered systems were found to be more effective than monolithic systems in reducing the damage that occurred due to high-

velocity impact loads. Therefore, a lot of studies have been conducted to examine the impact resistance of different kinds of multi-material systems made out of alloys, ceramics, foams, and polymers [3].

For example, Caminero et al. [13] conducted several studies to examine the resilience of carbon fiber-reinforced epoxy laminates to impact by incorporating low-velocity impact tests and Charpy impact tests. Experimental research was done on how laminate thickness and ply-stacking order affected the damage resistance of CFRP laminates under low-velocity impacts and concluded that thicker laminates absorb less energy compared to thinner laminates. Also, it was found that thicker laminates are more vulnerable to delamination due to their high bending stiffness.

Also, due to their exceptional qualities such as toughness, high strength-to-weight ratio, and high energy dissipation capability, composite materials have been found as an effective medium to mitigate the effect of impact loads [12]. However, despite the aforementioned advantages, those composite materials have their inherent drawbacks too. The residual characteristics and structural integrity of composite materials can be dramatically reduced by the invisible damages that occur due to impact loads. Also, a slight misalignment between the layers of the composite could cause delamination, which would greatly diminish its mechanical characteristics and impact resistance [14].

Chanel et al. [15] studied the potential of elastomer coating in impact damage mitigation for existing infrastructures and found its capability in retrofitting concrete structures. Also, double-skin composite structures that consist of a concrete core in between two steel plates were considered as one of the most effective impact resistance mechanisms due to the steel plates' tensile membrane resistance [16].

Rajendra [17] carried out several studies on auxetic-based structures as protective structures and found their superior protective performance due to high energy absorption capacity and lightness. Furthermore, functionally graded multi-material systems are also an area of interest due to their advantages such as enhancement of stress attenuation, robustness, and high preference for lightweight structures.

For decades, the development of high-performance protective structures against impact loads was inspired by the specific mechanical characteristics of biological

structures. It has been found that bio-inspired structures exhibit a remarkable improvement in energy absorption capacity and stress attenuation over conventional monolithic structures [18]. In bio-inspired designs, some of the characteristics and functions of biological organisms are incorporated into novel materials, and structures to ensure the anticipated characteristics [19]. As an example, multi-material 3D printed structures that surpass the impact-resistant capacities of monolithic materials have been inspired by the microarchitecture of seashell nacre [18].

In the past few years, researchers looked into the improved mechanical characteristics of nanoparticle-reinforced materials due to their distinctive properties. As an example, composites enhanced with Kevlar fabrics made out of high-modulus and high strength fibres have been found as a superior impact-resistance material. Also, Kevlar composites are highly used for lightweight armor structures [20]. Abdel et al. [12] studied the effect on the impact resistance capacity of a newly designed woven Kevlar KM2Plus/epoxy resin laminated composites enhanced with nanoparticles and nanotubes. Drop-weight impact tests were conducted to assess the impact resistance of the laminated composite reinforced with three different nanofillers including silicon carbide, aluminium oxide, and multi-walled carbon nanotubes.

As mentioned above, lots of innovative protective mechanisms against impact loads have been developed over the recent decades to be employed in different kinds of applications.

2.2 Numerical Modelling Approaches

Due to the ability of powerful computational tools to adopt the necessary geometrical and material parameters and perform virtual simulations at a quick rate, numerical modeling techniques are frequently utilized instead of physical tests and analytical models. However, to capture the nonlinearities of the impact problems in these numerical models, a significant number of material parameters must be identified and usually, those parameters are found by conducting actual experiments.

Over the years, several constitutive models have been developed to predict high-velocity impacts [21]. The most commonly used constitutive model was created by

Johnson and Cook for materials that experience significant strains, rapid strain rates, and high temperatures. Also, two additional stress models to simulate the plastic deformation of ductile materials were created by Zerilli [22] and Steinberg [23]. The material constants associated with those constitutive models and failure models are mainly determined using split Hopkinson-bar methods and universal tensile tests [24].

Ramirez [25] carried out a numerical study to simulate the wave propagation and scattering in the Hopkinson bar test based on finite element analysis. The Hopkinson bar test is one of the standard techniques for examining the mechanical characteristics of materials at high strain rates. The wave scattering that occurs in the incident bar alters the form of the pulse and limits the precision of the results. So, to mitigate the effect of wave dispersion on the output, a finite element simulation was carried out using the LS-DYNA FEA package and found that a trapezoidal pulse along with a high rise time decreases the wave dispersion and it could be obtained by positioning a disk or pad that can deform between the impactor and incident bar. In the finite element simulation, pad material was modeled using the Johnson-Cook constitutive equation and carried out a parametric analysis varying the material of the pad, diameter, and length which resulted in optimum characteristics for the deformable pad.

The utilization of sandwich structures against extreme loads has become popular due to their exceptional characteristics such as lightweightness and high energy absorption capacity compared to conventional materials. Guangyong et al. [26] did a combined experimental and numerical study to examine the dynamic behavior and failure processes of honeycomb sandwich panels that are impacted by a high-velocity spherical steel bullet. The numerical model of the honeycomb sandwich panel is shown in Figure 2.1.

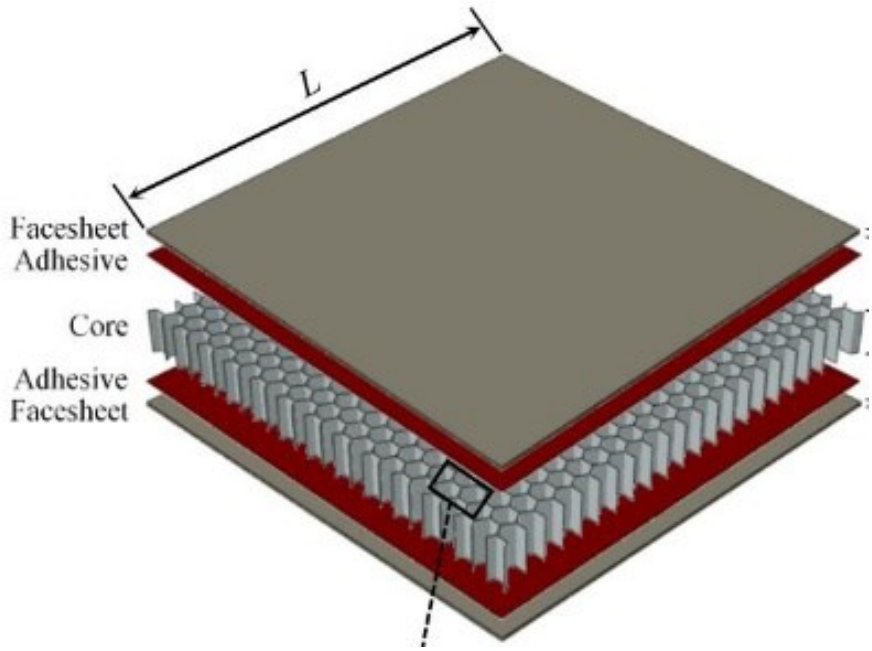

Figure 2.1 Schematic of honeycomb sandwich panel [26]

A 3D finite element (FE) model was developed in ABAQUS/Explicit which consists of a sandwich panel, projectile, and adhesive layers whose outputs were in good agreement with experimental results. The Johnson-Cook material model was used to define the nonlinear behavior of metallic face sheets and honeycomb cores. The developed numerical model was used to determine the critical perforation energy and ballistic limit velocity of sandwich panels.

Also, for the problems where conventional grid-based mesh approaches have difficulties due to the associated large distortions, a meshless Lagrangian numerical method has been developed by Gingold R. et al. [27]. This method has become a popular method for modeling impact-penetration issues in which large geometrical distortions occur.

Recently, Wenlong Yang [28] developed a coupled smoothed particle hydrodynamic (SPH) – finite element modeling (FEM) method to predict the anti-penetration performance of multi-layer composite structures under high-speed hemispherical-nosed projectiles as shown in Figure 2.2.

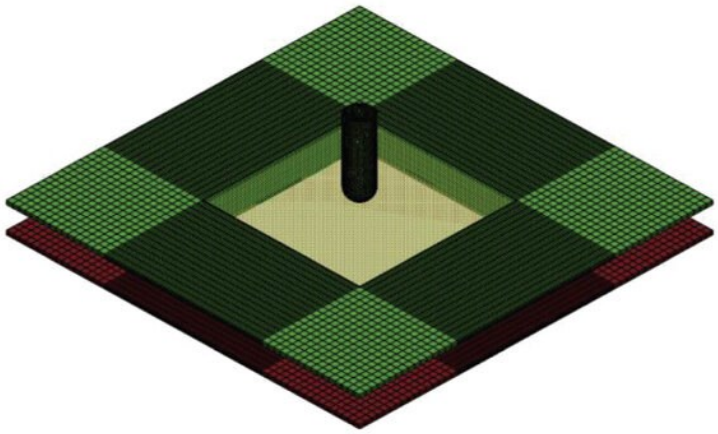

Figure 2.2 SPH-FEM model of composite target plates and hemispherical-nosed projectile [28]

When the FEM technique is used to simulate the penetration with high deformation of heterogeneous composite structures, issues such as element distortion are more prone to happen. However, in the proposed model, the SPH approach calculates the large deformation and broken areas, resolving the issue of element distortion in FEM. The FEM is utilized in other areas to enhance the efficiency of calculations. The results were compared against the experimental outputs and indicated that the developed coupled SPH-FEM model successfully predicts the ballistic limit and deformation accurately. In addition, studies and discussions on the deformation of different configurations including single-layer, multi-layer, and sandwich target plates with a core layer were carried out using the developed model. The coupled SPH-FEM method was identified as an effective alternative to address the associated problems in FEM such as element distortion during heterogeneous material penetration modeling.

A combined experimental and numerical study was done by Roy et al. [21] to predict the response of thick steel plates under hypervelocity projectile impact. The free surface velocity was measured experimentally using the Photonic Doppler Velocimetry (PDV) technique and those results were used to validate the numerical studies. Two different numerical approaches were developed incorporating the Johnson-Cook constitutive model and the MIE-Gruneisen equation of state: SPH and Eulerian-based hydrocode. Based on the area of physical damage and the

velocity histories of free surfaces, numerical simulations, and experimental results were compared which were found to be in good agreement. Therefore, the proposed numerical models were identified as a realistic alternative method for expensive experiments for projectile impact.

Fernando et al. [29] developed a more computationally efficient one-directional wave propagation rod model to study the potential of an impedance-graded metallic composite system in protecting a concrete structure against high-velocity impacts. The effect of impedance reduction between metallic materials on stress wave attenuation was explored and concluded that the magnitude of the transmitted wave would be reduced in a greater amount with a large impedance decrease.

Gio K et al. [30] investigated the mechanical behavior of aluminum foam sandwich plates under repeated impact loads by conducting both numerical and experimental studies. The foam core was modeled as solid elements while face sheets were as shell elements in ABAQUS. To define the contact between face sheets and the core, the numerical model shared the same nodes at the interface between them, and no specific contact was set. Due to the symmetry of the impact, the 3D model was simplified into 1/4 of the whole one. Also, to capture the large distortions in the impact zone, that area was refined into small finite elements compared to the rest of the area. To simulate the plastic crushable behavior of foam core, the Deshpande-Fleck constitutive model is employed.

Likewise, several attempts have been made to develop realistic numerical models to simulate the response of different materials under impact loads.

2.3 Analytical Modelling Approaches

Many studies have been carried out to develop realistic analytical models that are capable of simulating the behavior of different material systems under impact loads. Even though numerical models are found to be less complicated and easy to develop compared to analytical models, they also consist of some major drawbacks. For example, every FEA model has limited resolution even if the mesh is extremely fine. So, it might be an issue in this kind of study where stress waves have multiple interactions and reflections [7]. Also, numerical models are extremely expensive in terms of required computational power, compared to analytical models. Also, some

crucial outputs can be only obtained from analytical models and it is very difficult or almost impossible to obtain them from a numerical model. Therefore, several researchers carried out analytical studies to overcome the aforementioned disadvantages associated with numerical approaches.

Shock wave interaction and propagation have been broadly examined by Davison [31]. Mathematical representations have been given for uniaxial nonlinear plane longitudinal shock wave propagation based on three fundamental theorems, the balance of mass, momentum, and energy. The shock was identified as a discontinuous transition between two states, and the state of the material behind the shock and ahead of the shock was characterized by nine variables including density, stress, strain, particle velocity, and shock wave propagating velocity. Davison considered a discontinuous structured shock instead of a smooth transition between two states that could be found in real materials as shown below.

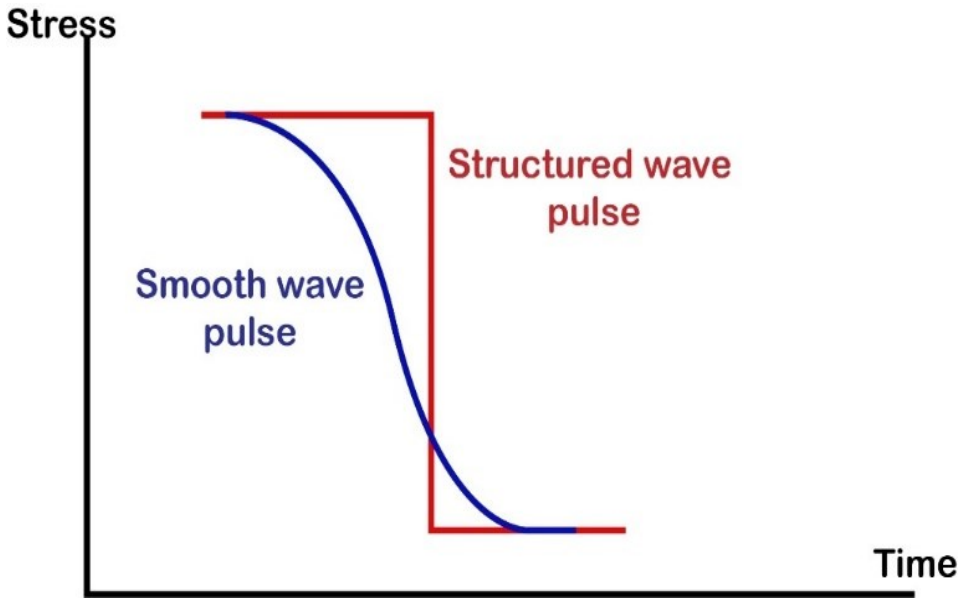

Figure 2.3 Smooth and structured wave pulses [31]

The aforementioned three conservation theorems are applicable to any material and contain no details on the differing responses of particular materials. So, Hugoniot relationships are taken into account to differentiate the material response from one to another. The curve that contains the achievable states by a material during a stress transition is known as the Hugoniot curve. It depends on the material state before the stress wave transition and it contains the specific characteristics of the material

studied. Davison L. presented a detailed explanation of different Hugoniots such as stress-volume, stress-particle velocity, and linear wave velocity-particle velocity. Also, solutions for different kinds of plane-shock interactions have been given including wave-boundary, wave-wave, and wave-material interface interactions. All shock interactions are calculated assuming that the longitudinal stress and particle velocity are equal on both sides of the interaction plane.

In several studies, homogenization techniques have been employed to simplify the shock response of multi-material systems. Agrawal V. et al [7] developed a solution for shock propagation through hypothetical material systems that were homogeneous to elastic waves but heterogeneous to shock waves. The yield strength, Young's modulus, and density are all the same for each material as shown in Fig 2.4. So, elastic waves pass through those material interfaces without any interaction However, because each material consists of different compressibility values, they are heterogeneous in terms of shock wave propagation. The typical stress-strain curve of realistic materials for extreme loads is described by an elastic linear region, followed by the Hugoniot limit, and then a convex increasing nonlinear response. In this study, this behavior was idealized into a piecewise affine curve as shown which made the problem simple for a detailed analysis.

Usually, the linear shock velocity vs. particle velocity Hugoniot is considered along with the momentum balance equation to solve the shock wave propagation. However, in this study, instead of that typical approach, an empirical relationship between stress and strain has been incorporated with a kinetic relationship that connects the shock speed to the rate of dissipation at the shock front which was developed by Knowles [32].

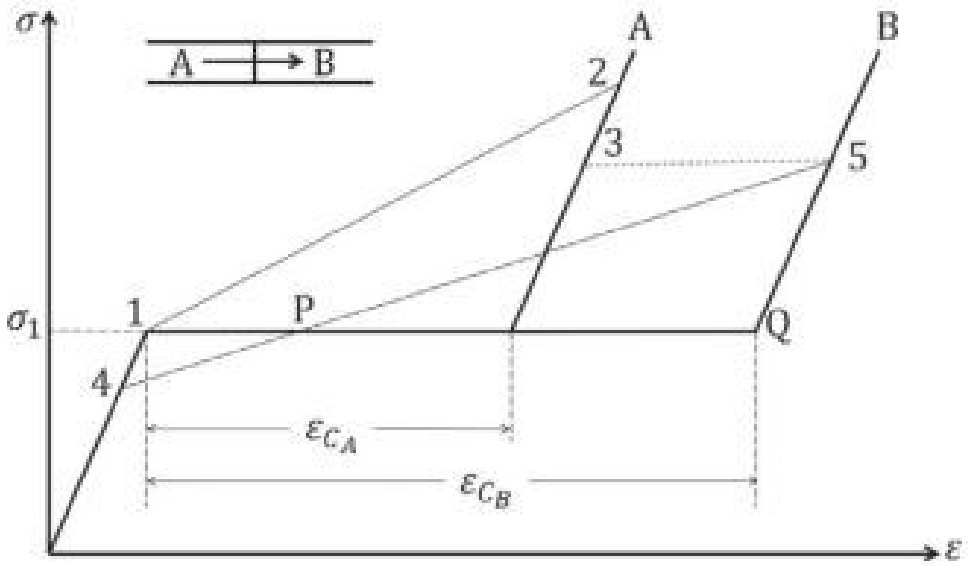

Figure 2.4 Idealized piecewise affine stress-strain curve [7]

Also, the structure of the shock was neglected, and it was treated as a discontinuity. The separation at material interfaces was not allowed as they were perfectly bonded. All possible wave interactions that could happen in a finite heterogeneous medium were cataloged along with their associated Reimann problems. Based on those interactions, an analytical model was implemented in MATLAB to find the response of the idealized heterogeneous medium. The developed model was used to study how the number of interfaces and their stiffness values affect the overall shock propagation phenomenon of a multi-material layered system and concluded that the amount of energy dissipation increases with the number of interactions. Also, it was found that material with numerous layers with gradual stiffness variation is preferred for stress mitigation to one with a sharp change in stiffness.

Satyendra P. et al. [1] developed a more generalized analytical model to predict the behavior of a layered medium with heterogeneous materials under one-dimensional impact loads by advancing the previously mentioned study. A multi-linear stress-strain curve that approximates the nonlinear stress-strain response was employed. However, the incorporated materials are heterogeneous for both elastic and shock waves. To determine the medium's response, a program was implemented that monitors and resolves the interactions of each wave that is propagating in the flyer-target system for three different cases: low velocity, intermediate velocity, and high-velocity collisions. By carrying out a finite element analysis using the ABAQUS

FEA package for the same problem, the impact behavior acquired from the analytical code was verified and agreed well for all three cases. Also, the developed model is capable of producing a distance vs time graph for stress wave propagation within the system. It gives a comprehensive idea of the wave interactions occurring as shown below in Fig 2.5.

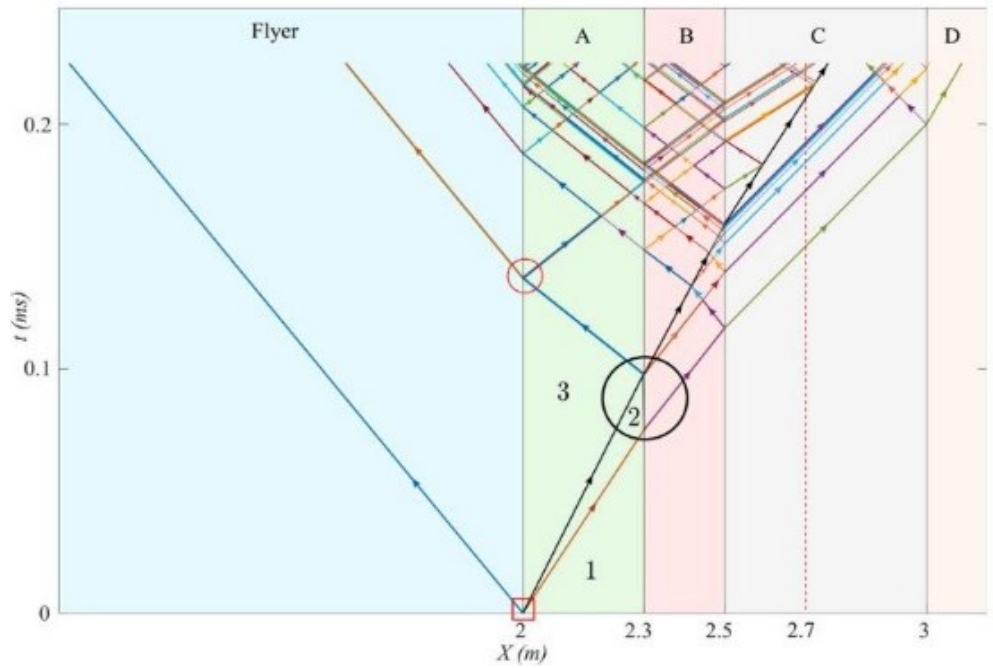

Figure 2.5 Distance-time plot for stress wave propagation through the layered material system [1]

Compared to the other analytical models in the literature, this model can be identified as a more generalized one as previous models are applicable only to periodic laminates and semi-infinite targets, and the separation of target and flyer is not allowed. However, even in this model, the separation of material plates is not allowed. Also, the idealization of the nonlinear stress-strain curve into a multi-linear stress-strain relation makes the developed model hypothetical.

Based on Floquet's theory of ordinary differential equations with periodic coefficients, an analytical approach was developed to address the one-dimensional wave propagation with high amplitudes in multilayer heterogeneous material systems [6]. The formulation of the problem was based on a typical plate impact experiment. The analytical model's findings are well consistent with both experimental data and the results of a shock wave-based finite element code.

Uniaxial shock wave propagation and interaction between waves and interfaces have been extensively studied in the book by Cooper W [33]. It includes a detailed description of shock waves including Rankine-Hugoniot jump equations, Hugoniot planes, interactions of shock waves, and rarefaction waves.

Likewise, several comprehensive analytical studies have been carried out to solve the problem of stress wave propagation in different kinds of material systems. In the majority of them, various assumptions have been made to simplify the problem and make it trackable analytically. In most of them, the nonlinear stress-strain curve was simplified into a multi-linear relationship. Also, no study has been done on higher dimension wave propagation and only one-dimensional wave propagation has been considered. Also, it is worth mentioning that, the calculation of the amount of energy dissipation during wave propagation and interaction is almost impossible using the balance equations mentioned above. And, no analytical approaches have been developed to address the oblique impacts. This means that the applicability of the developed analytical models is very limited compared to numerical models and they are valid only for some idealized cases which are far away from the real-world scenarios.

2.4 Research Gaps

After conducting the above literature review, the following research gaps were identified. In some analytical models developed in previous studies, the non-linear behavior of the stress-strain curve above the HEL value has been neglected. Instead of that, an idealized piecewise linear stress-strain relationship has been considered for the convenience of analysis. However, in this study, the non-linear stress-strain relationship during high strain rates was taken into account.

Also, in most of the studies, it is not allowed to separate layered materials at interfaces, even though tensile stresses are generated at material interfaces. So, that type of model cannot be used to calculate the required bonding strength to avoid debonding at material interfaces. So, in the current study, the bonding strength between layered materials was taken as zero which allows the separation of metallic plates under tensile stresses.

Furthermore, in several studies, analytical models have been developed for infinite

or semi-infinite heterogeneous layered systems. In those models, the effect of free surfaces/ boundaries on overall stress wave propagation cannot be studied. They only facilitate the wave interactions at material interfaces. However, in real-world applications, infinite or semi-infinite systems cannot be found, and therefore, in this study, finite multi-layered systems were taken into account.

Also, some 3D numerical models developed in previous studies are not computationally efficient. As well as Lagrangian-based FEM models result in excessive mesh deformations under extreme loads. Therefore, a computationally efficient 2D axisymmetric numerical model was developed considering the symmetry of the impact.

Likewise, the current study was carried out to address these research gaps and come up with a more generalized analytical and numerical model.

3 NUMERICAL MODELLING OF MULTI-METALLIC LAYERED TARGETS

As mentioned earlier, this study consists of two major components. 1) Elastic wave propagation and 2) Shock wave propagation. For both components, the specific metallic plate configurations were selected to match the available experimental results. For elastic wave propagation, four different test cases were considered including steel (S) monolithic target, steel-titanium (ST) and steel-aluminium (SA) bi-metallic targets, and steel-titanium-aluminium (STA) tri-metallic target as shown in Table 3.1.

Table 3.1 Test configuration for elastic wave propagation

Test Case		1	2	3	4
		S	ST	SA	STA
Impactor	Diameter	60 mm	60 mm	60 mm	60 mm
	Thickness	6 mm	6 mm	6 mm	6 mm
	Material	Aluminium 2	Aluminium 2	Aluminium 2	Aluminium 2
Target	Diameter	60 mm	60 mm	60 mm	60 mm
	Total thickness	6 mm	6 mm	6 mm	6 mm
	Material 1	Steel	Steel	Steel	Steel
	Thickness	6 mm	3 mm	3 mm	2 mm
	Material 2	-	Titanium	Aluminium 1	Titanium
	Thickness	-	3 mm	3 mm	2 mm
	Material 3	-	-	-	Aluminium 1
	Thickness	-	-	-	2 mm

A flyer velocity of 180 ms^{-1} was selected for elastic wave propagation to be consistent with the available experimental results. Two different types of Aluminium were used for the flyer (Aluminium 2) and the target (Aluminium 1).

However, for shock wave propagation, only a steel monolithic test case was considered as shown in Table 3.2. A flyer velocity of 350 ms^{-1} was selected for shock wave propagation to be consistent with the available experimental results.

Table 3.2 Test configuration for shock wave propagation

	Diameter	Thickness	Material
Impactor	60 mm	6 mm	Steel
Target	60 mm	6 mm	Steel

3.1 Material Properties

In a non-rigid body, dilatation and distortion take place as stresses build. The total stress generated in a material during high-strain rates can be divided into two subsets for the convenience of analysis; (1) Hydrostatic stress which is also known as dilatational stress and (2) deviatoric stress. The uniform displacement of particles over a solid, toward or away from one another, is known as dilation due to hydrostatic stress and it is mainly responsible for volume change. In contrast, differential particle displacement occurs across the material as a result of distortion due to the deviatoric stress, and it is related to shape change [24]. Deviatoric stress is essential to take into account when the plastic behavior of a solid is concerned as deviatoric stress is the kind of stress component that is responsible for yielding. Hydrostatic stress can be simply denoted by the average of three principal stresses of any stress tensor (Eq. 3.1) where σ_{11},σ_{22}, and σ_{33} are principal stresses, and it does not include any shear components.

$$\sigma_H = \frac{\sigma_{11}+\sigma_{22}+\sigma_{33}}{3} \qquad 3.1$$

After deducting the hydrostatic stress from the total stress tensor, the remaining

stress is known as the deviatoric stress as shown by Eq. 3.2.

$$\begin{bmatrix}\sigma_{11} & \sigma_{12} & \sigma_{13}\\ \sigma_{21} & \sigma_{22} & \sigma_{23}\\ \sigma_{31} & \sigma_{32} & \sigma_{33}\end{bmatrix} - \begin{bmatrix}\sigma_H & 0 & 0\\ 0 & \sigma_H & 0\\ 0 & 0 & \sigma_H\end{bmatrix} = \begin{bmatrix}\sigma_{11}-\sigma_H & \sigma_{12} & \sigma_{13}\\ \sigma_{21} & \sigma_{22}-\sigma_H & \sigma_{23}\\ \sigma_{31} & \sigma_{32} & \sigma_{33}-\sigma_H\end{bmatrix} \quad 3.2$$

When materials are subjected to extreme dynamic loads such as impacts and blasts, they are anticipated that they will undergo high strain rates generating both volume and shape changes. In this study, the MAT_JOHNSON_COOK constitutive material model and the GRUNEISEN Equation of State (EOS) were used to take into account the deviatoric and hydrostatic stresses respectively.

3.1.1 JOHNSON-COOK Constitutive Material Model

Under large deformations, high strain rates, and high temperatures, the Johnson-Cook model can be utilized to characterize the relationships between stress and strain in metallic materials. Due to its simple form and the ease with which the material constants can be estimated, it is being widely used to simulate the behavior of materials in both research and industrial works [24]. The stress model can be expressed by Eq. 3.3. σ and ε refer to the equivalent stress and the equivalent plastic strain respectively where A, B, n, C^*, and m are material constants and they refer to the yield stress of the material under reference conditions, the strain hardening constant, the strain hardening coefficient, the strengthening coefficient of strain rate, and the thermal softening coefficient respectively [23]. T is for temperature in Kelvin degrees.

$$\sigma = (A + B\varepsilon^n)(1+C^* \ln\varepsilon^*)(1-T^{*m}) \quad 3.3$$

The three main components of Eq. 3.3; $(A + B\varepsilon^n)$, $(1+C^* \ln\varepsilon^*)$, and $(1-T^{*m})$ represent the strain hardening effect, the strain rate strengthening effect, and the temperature effect respectively that affect significantly the stress values [34]. In the model, ε^* represents (Eq. 3.4) the dimensionless strain rate and T^{*m} (Eq. 3.5) is the homologous temperature.

$$\varepsilon^* = (\text{Strain rate}/\text{ reference strain rate}) \quad 3.4$$

$$T^{*m} = \frac{(T - T_{ref})}{(T_{melt} - T_{ref})} \quad 3.5$$

T_{melt} is the temperature at which melt occurs of that particular material considered and T_{ref} can be selected according to the problem. However, the previously mentioned material models should be selected in accordance with the reference conditions. Numerous experiments have been carried out using Split Hopkinson-bar tests and universal tensile tests at elevated temperatures and strain rates to identify the Johnson-Cook material model parameters for various materials. In this study, material parameters for steel, titanium, and aluminium were extracted from previous experimental studies.

Table 3.3 Johnson-Cook material model parameters

Material Parameter	Steel [35]	Titanium [36]	Aluminium 2 [37]	Aluminium 1 [38]
A (MPa)	1500	900	270	520
B (MPa)	1965	510	154	477
n	0.4	0.506	0.222	0.520
C^*	0.003	0.03	0.13	0.0025
m	1	1	1.34	1.61
Reference strain rate (/s)	1	1	600	0.0005

In this study, two different Aluminium types were incorporated; 6061-T6 (Aluminium 2) and 7075-T651(Aluminium 1). Therefore, Johnson-Cook material model parameters vary from one to another.

3.1.2 Equation of States (EOS)

An equation of state is a mathematical relationship that expresses how a physical system will behave in terms of its thermodynamic characteristics such as temperature, volume, and pressure. It is mainly used to describe the response of a material under different physical conditions. In this study, GRUNEISEN EOS was used to take into account the hydrostatic pressure with the parameters C_B and S1 for bulk sound speed and linear Hugoniot slope coefficient respectively. S2 and S3 are higher-order coefficients of the Hugoniot that are used to obtain highly accurate predictions. However, in this study, a simplified linear relationship was used without considering higher-order coefficients.

In the analysis of shock compression in several common solids within the pressure range of several hundred GPa, the Gruineisen equation of state is frequently used [31]. It relates the pressure and volume of a solid at a given temperature and is used to calculate the pressure in a solid that has been compressed by a shock [39]. Parameters of EOS are generally found through plate impact experiments at different flyer velocities.

Table 3.4 Gruneisen EOS parameters

Material Parameter	Steel [35]	Titanium [36]	Aluminium 2 [37]	Aluminium 1 [38]
C_B (m/s)	4569	5130	5240	5240
S1	1.490	1.028	1.400	1.400
S2	0	0	0	0
S3	0	0	0	0
Gruneisen parameter	2.17	1.23	1.97	1.97

3.2 Development of 2D Axisymmetric Models

To reduce the required computational power, the actual 3D case was idealized into a 2D axisymmetric model since the impact event is symmetric in terms of loads and geometry about the center line of the target plates. It facilitated to obtain a significant mesh refinement that ensured the accuracy of the captured stress variations. To ensure the idealized 2D model represents the actual 3D model, the flyer and target materials were modeled using the shell element SECTION_SHELL with the use of element formulation 14 [40]. It is an 'axisymmetric solid–area weighted' model and the global y-axis is taken as the axis of symmetry for axisymmetric element formulations in LS_DYNA by default. Even though it is a 2D model the effect of the transverse waves which get reflected at the perimeter and propagate back into the target can be simulated. The idealization is shown in Fig. 3.1.

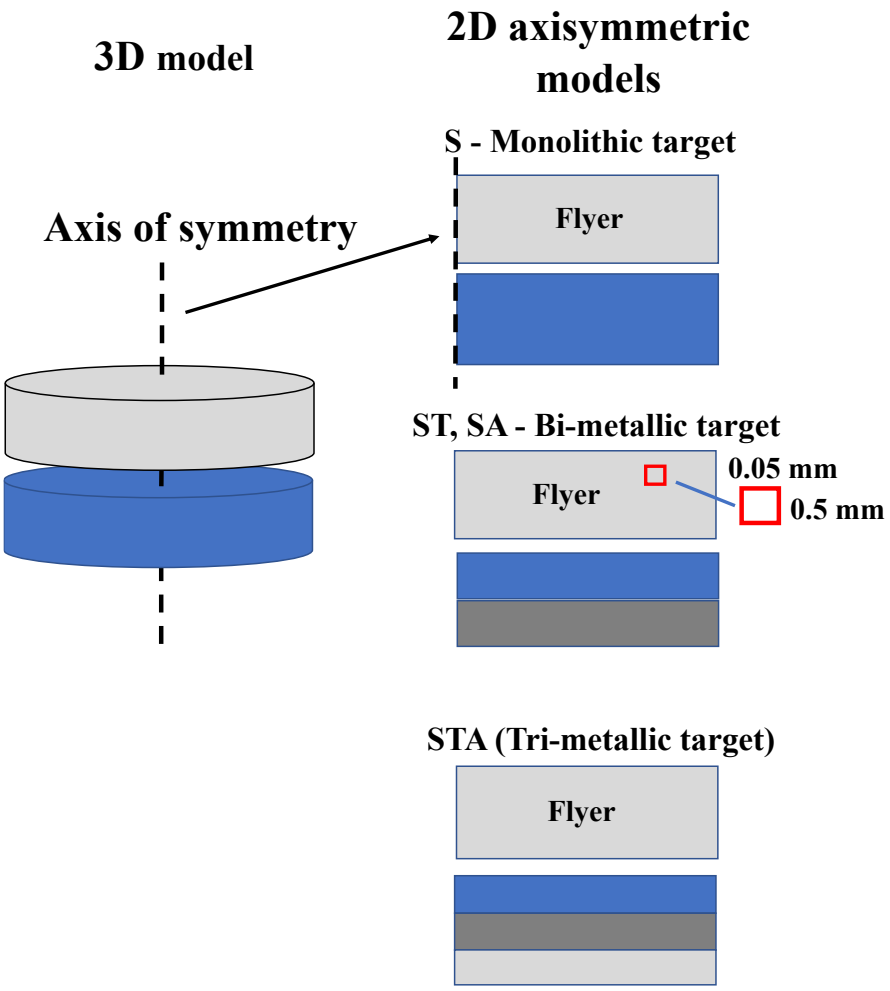

Figure 3.1 2D axisymmetric FEM model

3.3 Enforcement of Boundary Conditions

Because of the exceptional speed of the impact, only the uniaxial state of strain behavior was expected along the Y-axis. Also, no inplane (about the Y axis) or out-of-plane rotations (about the X or Z axes) can be expected due to the rigidity of metallic plates. Since the metallic target was kept within a steel ring during the experiment, the target was assumed to be radially fixed. So, the translation along the X axis was constrained. In that way, all the rotations, and translations along the X and Z axes were constrained. Even though the constraint on translation along the X-axis might affect the stress generation along the X direction, only one-dimensional stress variation along the Y-axis is the topic of interest.

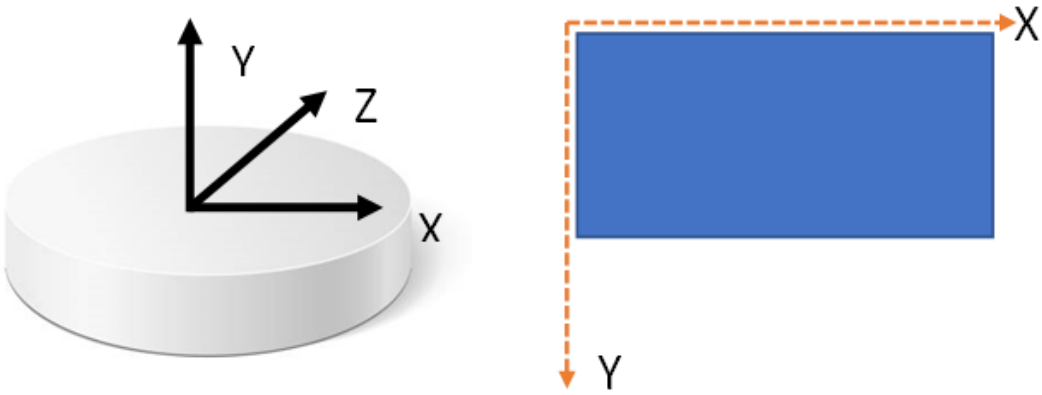

(a) (b)

Figure 3.2 (a) 3D case (b) 2D axisymmetric model

The keyword 'BOUNDARY_SPC_SET' was used to define the boundary conditions.

3.4 Contact of Material Interfaces

In LS_DYNA, the keyword 'CONTACT' is used to define the interaction between disjoint parts. Based on the type of interaction, different kinds of contacts have been given for 3D contacts and 2D contacts. 'CONTACT_2D' is the general contact algorithm for 2D cases.

Generally, the automatic contact options are employed when predetermination of contact that takes place is difficult or impossible. Automatic contacts are non-oriented and they can identify penetration coming from either side of a shell element. Therefore, in this study, the 'CONTACT 2D AUTOMATIC SURFACE TO

SURFACE' contact card was employed to guarantee the transfer of stress between different parts in the multi-metallic targets including the flyer.

Mainly there are two different contact types based on the process of checking slave nodes for penetration. 1) One-way treatment of contact and 2) Two-way treatment of contact. In the former, penetration through the master segments is checked for only the user-specified slave nodes. However, in the second one, the penetration is checked for both slave nodes and master nodes through the master segment and slave segment respectively. Therefore, the treatment is symmetric and the slave node and master node can be defined arbitrarily. The contact card 'CONTACT 2D AUTOMATIC SURFACE TO SURFACE' is a two-way treatment contact and therefore, in the current study, the metallic plates and flyer can be defined randomly for slave and master segments.

3.5 Mesh Sensitivity Analysis

A mesh sensitivity analysis was carried out to find the required mesh refinement to have the mesh size smaller than the wavelengths of the stress waves [40]. The steel-titanium (ST) test case was considered and the initial incident stress, the reflected and transmitted stresses at the steel-titanium interface were considered as shown in Fig 3.3. The initial incident stress and reflected stress were measured at an element at the center of the steel plate while the transferred stress was measured at an element at the center of the titanium plate.

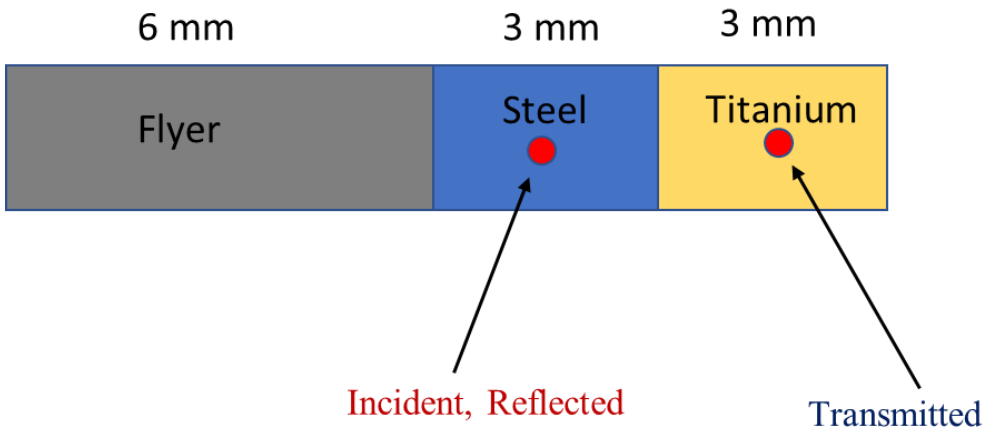

Figure 3.3 Selected elements for mesh sensitivity analysis

The initial mesh size of the finite elements in both flyer and target plates was 0.6

mm and gradually reduced up to 0.02 mm. Consequently, the number of elements in the entire flyer-target system increased from 1000 to 0.9 million. It was shown that the stress values become constant for mesh sizes smaller than 0.05 mm as shown in Fig. 3.4. Hence, for all the numerical models, a mesh size of 0.05 mm × 0.05 mm was used. Here the efficiency of a two-dimensional model in terms of required computational power is obvious since a three-dimensional model with this level of mesh refinement would consist of a large number of elements which leads to a high computational cost. To obtain a smooth variation in stress-time histories, the time interval between outputs was selected as 20 ns.

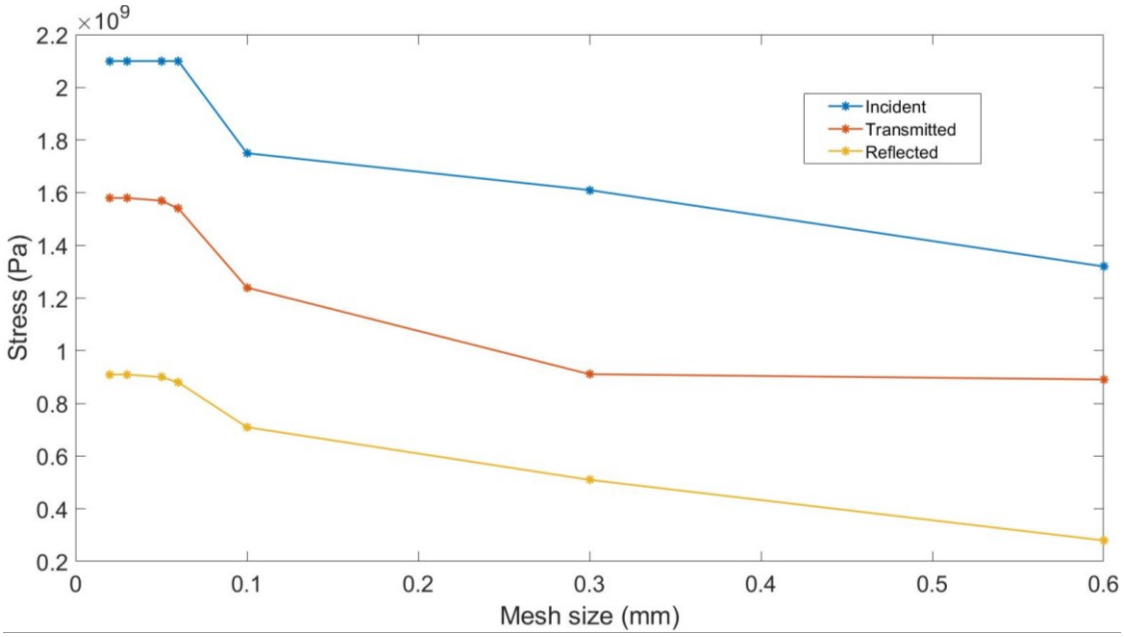

Figure 3.4 Mesh sensitivity analysis

As shown in Fig. 3.4, the stress values for the incident, transmitted, and reflected waves remain steady at a constant value of 2.1, 1.6, and 0.9 GPa respectively for mesh sizes smaller than 0.05 mm.

4 DEVELOPMENT OF THE ANALYTICAL MODEL

4.1 Material Response for Extreme Loads

High-velocity impacts result in high pressures and strain rates in materials, which generate stress waves (elastic and/or shock waves). When a stress wave travels through a heterogeneous medium, it interacts with the boundaries and material interfaces, changing the state of the system [31]. In high-velocity impact events, materials operate in the hydrodynamic domain when the strain rate is equal to or higher than 10^4/s [41]. Materials that are in a hydrodynamic regime behave like compressible viscous fluids and cause stress waves to propagate through them.

The type of stress waves propagating through a material during a high-velocity impact depends on the HEL of that material and the magnitude of the stress wave. The HEL is given by the Eq. 4.1 where Y_d refers to the dynamic yield strength under uniaxial stress conditions, and v is Poisson's ratio of the material. When the magnitude of a generated wave exceeds the material's HEL value, there would be a shock wave along with a foregoing elastic wave. Otherwise, there would be only an elastic wave.

$$\text{HEL} = \frac{1-v}{1-2v} Y_d \qquad 4.1$$

Simply, a stress wave can be identified as a moving surface where the displacement is continuous while other field variables such as mass density, particle velocity, stress, and strain are discontinuous. A stress wave splits the material in which it is traveling into two parts [31]. (1) Upstream material (2) Downstream material. The material's upstream state can be described by the four variables $S^1 = (\sigma^1, \varepsilon^1, \upsilon^1, \rho^1)$ while $S^0 = (\sigma^0, \varepsilon^0, \upsilon^0, \rho^0)$ for downstream material. σ, ε, υ, ρ represent stress, strain, particle velocity, and density respectively. The description of the wave is complete once the shock velocity (U) is known.

4.2 Governing Equations

The mechanical behavior of a material under extreme loads is governed by the fundamental principles of energy conservation, mass conservation, and momentum conservation [31]. The mass, momentum, and energy balance equations yield the jump equations Eq. 4.2, Eq. 4.3, and Eq.4.4 respectively in the Lagrangian form that

relate the aforementioned field variables. In Eq. 4.4, 'e' is referred to specific internal energy and it can be denoted as the addition of strain energy per unit mass and kinetic energy per unit mass as shown in Eq. 4.5.

$$(\varepsilon^1 - \varepsilon^0)U + \upsilon^1 - \upsilon^0 = 0 \quad 4.2$$

$$(\sigma^1 - \sigma^0) + \rho U(\upsilon^1 - \upsilon^0) = 0 \quad 4.3$$

$$\rho(e^1 - e^0) - \frac{1}{2}(\sigma^1 + \sigma^0)\left(\frac{1}{\rho_0} - \frac{1}{\rho_1}\right) = 0 \quad 4.4$$

$$e = \int \rho\left(\varepsilon + \frac{\upsilon^2}{2}\right)du \quad 4.5$$

Usually, the state ahead of a stress wave (S^0) is known, and then there will be only five unknowns. The three jumping equations reduced it to two unknowns and the stimulus which produces the stress wave is usually defined by a boundary condition (one of the upstream variables). An additional equation is required to determine the remaining unknown field variable and that is where Hugoniot constitutive relations come into play.

For simplicity, the problem is assumed as isothermal. Therefore, the temperature in the system remains constant and the thermal equilibrium is maintained because the system's heat transmission occurs so slowly. Hence, the energy balance equation (Eq. 4.4) does not need to be considered. Hence, the governing equations reduce to the jumping equations Eq. 4.2 and Eq. 4.3. However, due to this assumption, it does not allow to calculate the energy dissipation that occurred during wave propagation. This study mainly considered the stress and particle velocity variation over time under the given impact event. Therefore, Eq. 4.3 which describes the relation between stress and particle velocity was taken into account along with the shock and particle velocity Hugoniot. There is no specific information in the aforementioned three jump equations that characterizes the differing responses of the material considered. However, the Hugoniot contains the characteristics of the considered material and it varies with that specific material. Also, it depends on the initial state (S^0). Eventually, the governing equations can be reduced to the Eq. 4.3 and Eq. 4.6 where C_B is referred to the material's bulk wave speed and S is the linear Hugoniot slope coefficient.

$$U = C_B + S(\upsilon^1 - \upsilon^0) \quad 4.6$$

4.2.1 Elastic Wave Propagation

However, when it comes to elastic wave propagation, longitudinal wave velocity (U) is constant for a given material. So, the elastic wave propagation can be solved by using only Eq. 4.7 as shown. The longitudinal elastic wave propagation velocity is given by the fundamental Eq. 4.8 where E refers to Young's modulus of the material.

$$(\sigma^1 - \sigma^0) + \rho C(\upsilon^1 - \upsilon^0) = 0 \quad 4.7$$

$$C = \sqrt{E/\rho} \quad 4.8$$

4.2.2 Shock Wave Propagation

When shock waves propagate through a material, the wave velocity also varies with the initial conditions. By substituting Eq. 4.6 into Eq. 4.3, the following governing equation, Eq. 4.9 that describes the shock wave propagation can be obtained.

$$(\sigma^1 - \sigma^0) + \rho C(\upsilon^1 - \upsilon^0) + \rho S(\upsilon^1 - \upsilon^0)^2 = 0 \quad 4.9$$

4.3 Plain Stress Wave Interaction

When a stress wave propagates through a multi-material system, there might be three different types of interactions; (1) wave-interface, (2) wave-free surface, and (3) wave-wave interaction. An interaction at a free surface generates only a reflected wave while wave-wave or wave-interface interactions generate both transmitted and reflected waves. The foundational concept of calculation of all stress wave interactions is that the stress and particle velocity components are the same on both sides of the plane of interaction which is known as compatibility. Therefore, the equilibrium state at the plane of interaction can be determined by obtaining the intersection of the corresponding stress vs. particle velocity Hugoniots as shown below.

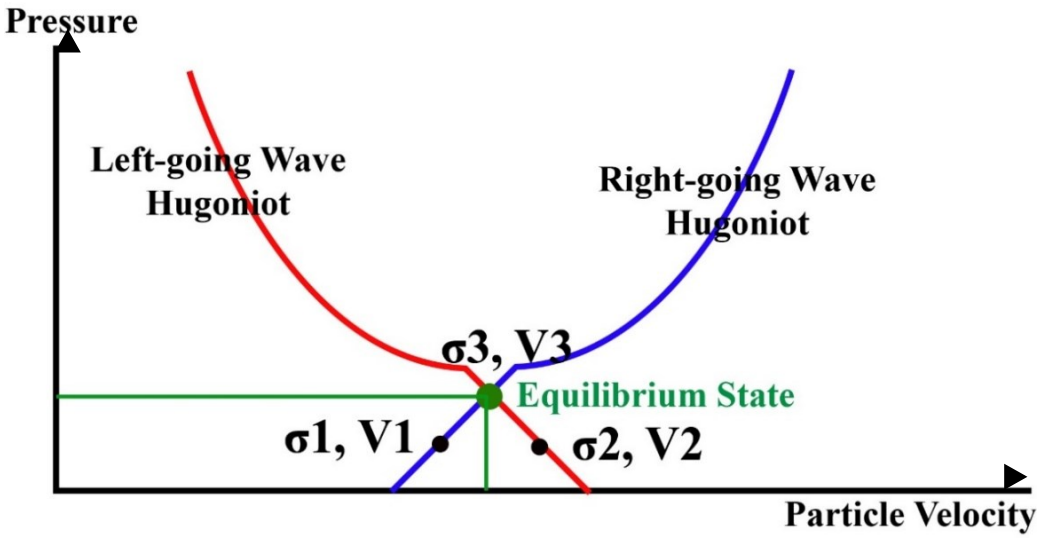

Figure 4.1 Intersection of right-going and left-going wave Hugoniots

When a stress wave interacts with a boundary/ free surface, the reflected wave takes the material into a stress-free state. The resultant particle velocity at the free surface depends on both the particle velocity of the free surface before the interaction and the particle velocity of the interacted wave as shown below.

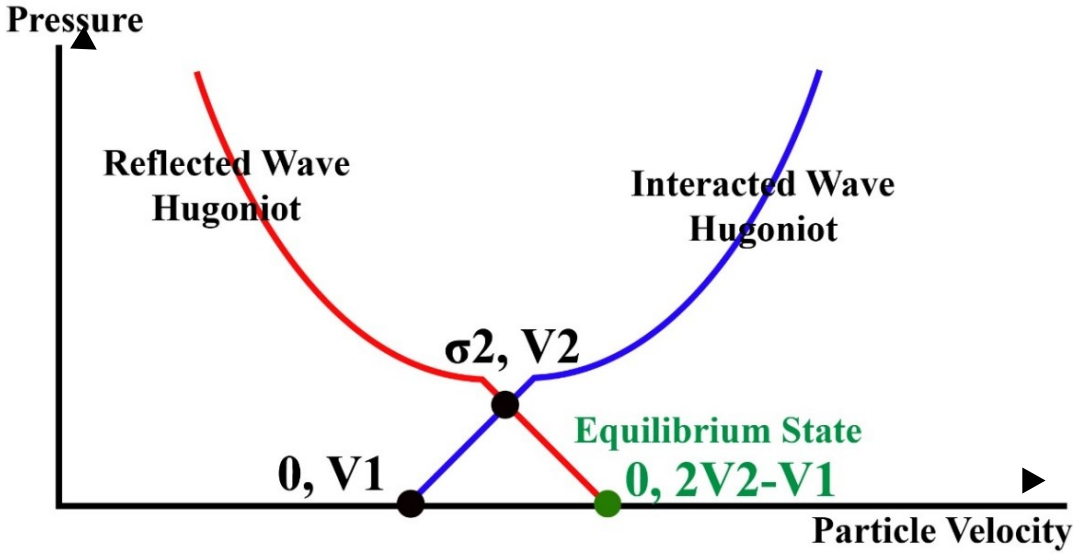

Figure 4.2 Resultant particle velocity of a reflected wave at the free surface

4.3.1 Elastic Wave Interaction

The interaction of elastic waves can be easily solved analytically as the wave velocity does not vary with the stress magnitude. This section describes the associated Reimann problems for elastic wave interaction with an interface formed by two different materials and elastic wave interaction with another elastic wave as

shown in Fig 4.3 and Fig. 4.4 respectively.

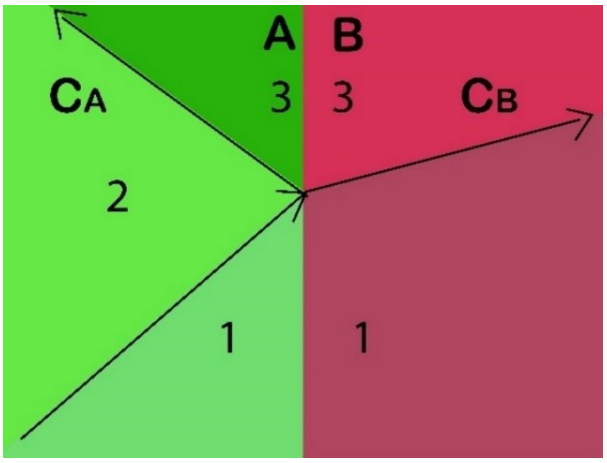

Figure 4.3 Elastic wave interaction with an interface

$$(\sigma_3 - \sigma_1) + \rho_B C_B(\upsilon_3 - \upsilon_1) = 0 \qquad 4.10$$

$$(\sigma_3 - \sigma_2) - \rho_A C_A(\upsilon_3 - \upsilon_2) = 0 \qquad 4.11$$

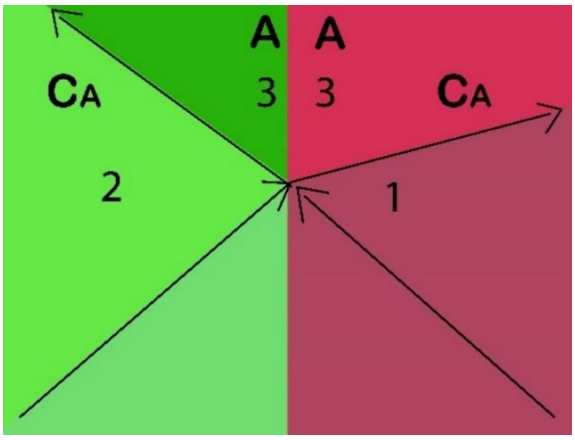

Figure 4.4 Elastic wave interaction with another elastic wave

$$(\sigma_3 - \sigma_1) + \rho_A C_A(\upsilon_3 - \upsilon_1) = 0 \qquad 4.12$$

$$(\sigma_3 - \sigma_2) - \rho_A C_A(\upsilon_3 - \upsilon_2) = 0 \qquad 4.13$$

As shown in Fig. 4.3 and Fig. 4.4, equilibrium stress states are denoted by 1,2 and 3 after propagating corresponding stress waves. By compatibility, both materials are in the same stress state with the same particle velocity at the plane of interactions. σ_3 and υ_3 are variables in the set of equations. As shown in Fig. 4.3, the forward

elastic wave changes the equilibrium state of material B from state 1 to state 3 and is represented by Eq. 4.10. The backward elastic wave takes the equilibrium state of material A from state 2 to 3 and is represented by Eq. 4.11. It is worth mentioning that, since wave-wave interaction occurs inside a material, 'ρ' and 'C' should be the same for both equations for a wave-wave interaction. In this notation, compressive stresses and right-going wave speeds are considered positive.

4.3.2 Shock Wave Interaction

Compared to elastic wave analysis, shock wave analysis is slightly more challenging as the wave velocity varies with the stress generated. Therefore, as mentioned earlier, an empirical equation of wave velocity vs. particle velocity (Hugoniot) should be combined with the equation obtained from the momentum conservation. Eq. 4.9 which describes the shock wave propagation can be simplified further to Eq. 4.14 if the particle velocity (υ^a) corresponding to zero stress is known.

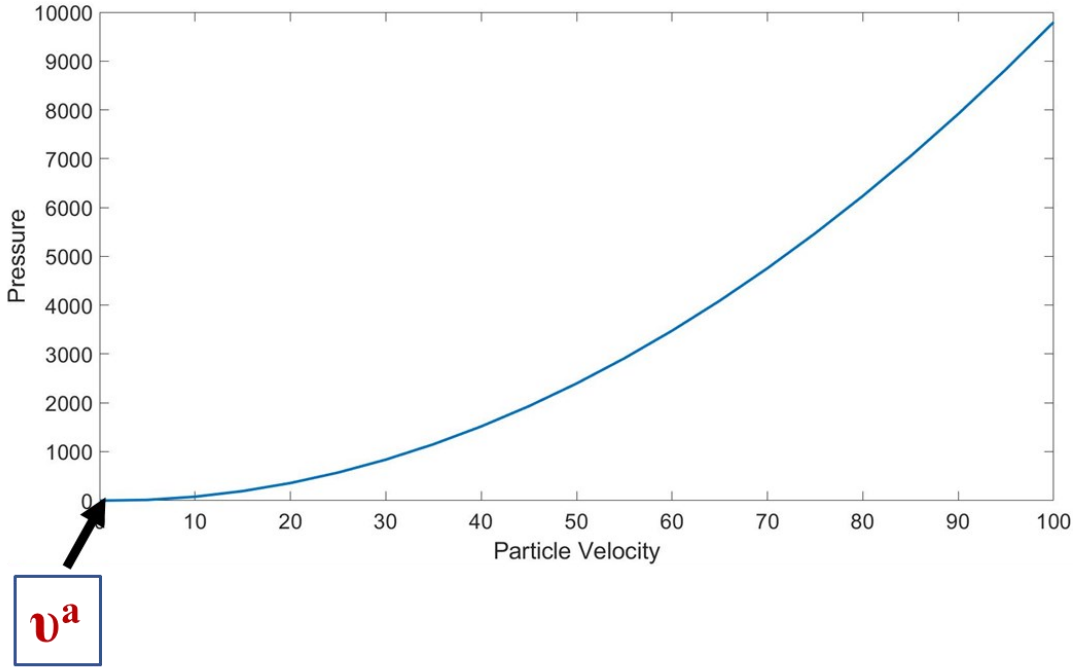

Figure 4.5 Graphical representation of the simplified shock wave propagation equation

$$\sigma^1 = \rho C(\upsilon^1 - \upsilon^a) + \rho S(\upsilon^1 - \upsilon^a)^2 \qquad 4.14$$

So, by the compatibility, it is known that both pressure and particle velocity will be the same at the interaction plane if the two materials remain in touch after the interaction. So, the solution can be found simply by setting to be equal the Hugoniots

of right-going (Eq. 4.15) and left-going (Eq. 4.16) waves as shown where υ^a and υ^b are the particle velocities of right-going and left-going Hugoniots corresponding to zero stress.

$$\sigma^1 = \rho_A C_A(\upsilon^1 - \upsilon^a) + \rho_A S_A(\upsilon^1 - \upsilon^a)^2 \quad 4.15$$

$$\sigma^1 = \rho_B C_B(\upsilon^b - \upsilon^1) + \rho_B S_B(\upsilon^b - \upsilon^1)^2 \quad 4.16$$

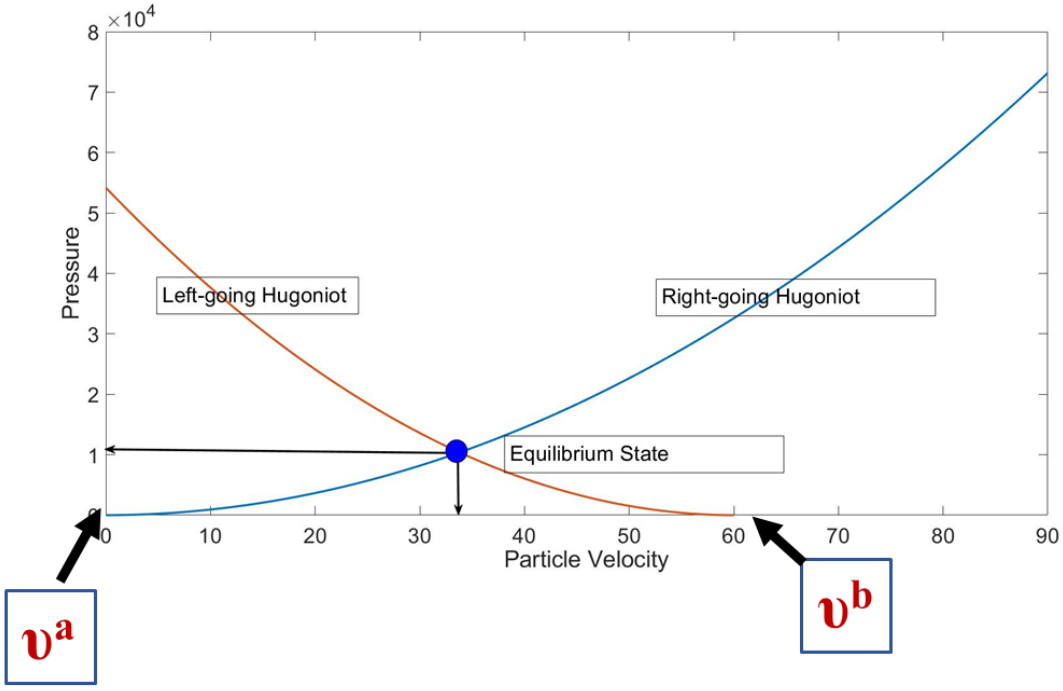

Figure 4.6 P-V Hugoniots for Right-going and left-going shock waves in materials with negligible strength

However, the aforementioned equations have been developed for a material with negligible strength. In these materials, the stress is equivalent to only the hydrodynamic pressure where deviatoric pressure is not taken into account. However, real materials consist of their inherent strength. Therefore, beyond the HEL, the actual pressure vs. particle velocity Hugoniot (Curve A) should lie 2/3 Y above the hydrodynamic curve (Curve B), which describes the response of a material with negligible strength [42] as shown in Figure 4.7.

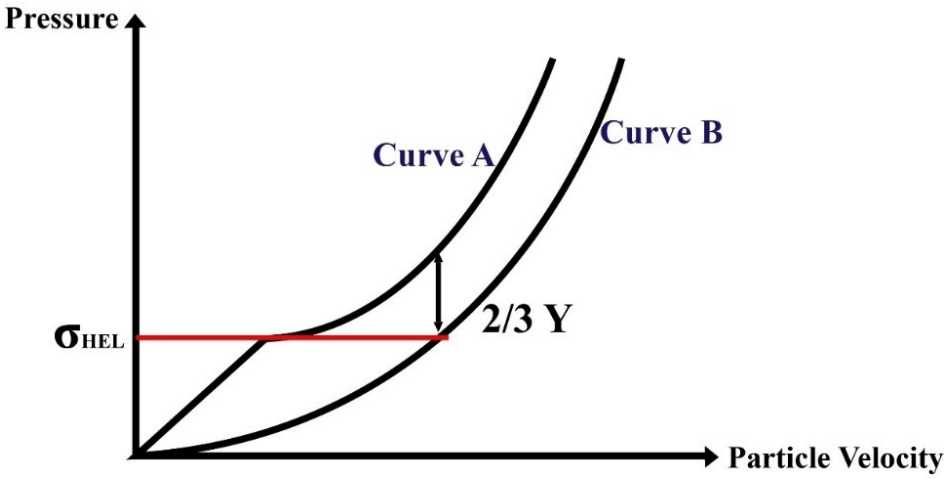

Figure 4.7 P-V Hugoniot for a material with negligible strength (curve B) and a material with strength (curve A)

Accordingly, the governing equations for shock wave propagation can be modified as shown below.

$$\sigma_{\text{right-going}} = \rho_A C_A(\upsilon^1 - \upsilon^a) + \rho_A S_A(\upsilon^1 - \upsilon^a)^2 + \frac{2}{3}Y_1 \qquad 4.17$$

$$\sigma_{\text{left-going}} = \rho_B C_B(\upsilon^b - \upsilon^1) + \rho_B S_B(\upsilon^b - \upsilon^1)^2 + \frac{2}{3}Y_2 \qquad 4.18$$

4.4 Modified P-V Hugoniot Curve for Shock Wave Propagation

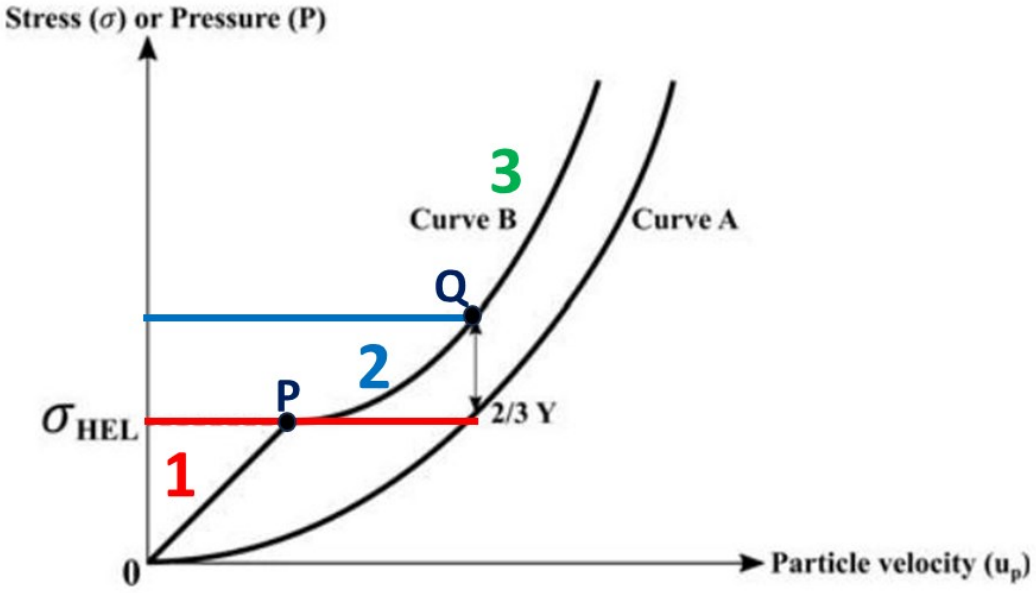

Figure 4.8 Modified P-V Hugoniot Curve for Shock Wave Propagation

The region below the HEL (region 1), which is known as the Elastic region can be simply defined by Eq. 4.19.

$$\sigma^1 = \rho C(\upsilon^1 - \upsilon^0) \qquad 4.19$$

However, region 2 in the stress-strain curve cannot be represented by the previously mentioned Eq. 4.17 which is for shock wave propagation and is only valid for region 3. Therefore, an alternative quadratic function that represents region 2 should be developed. However, there are only two known points (P and Q). Therefore, only a linear function can be derived instead of a quadratic function.

By following the above procedure, the governing equations for all three regions were derived for both right-going and left-going stress vs. particle velocity Hugoniots. Eq. 4.20, Eq. 4.21, and Eq.4.22 represent regions 1,2, and 3 of the right-propagating wave respectively in steel.

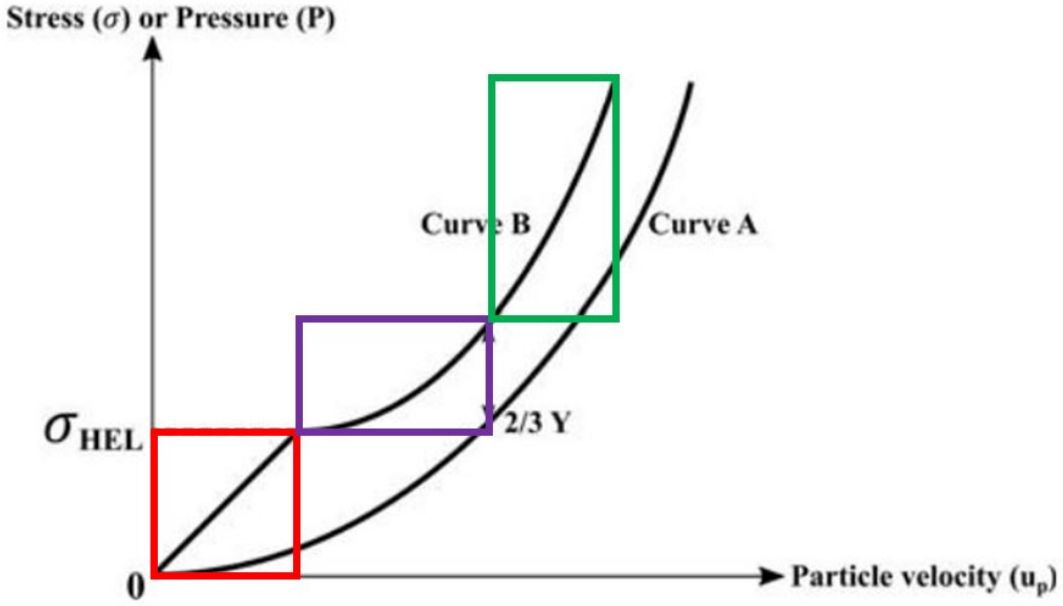

Figure 4.9 Modified P-V Hugoniot curve for right-going shock wave

$$\sigma^1 = 0.041(\upsilon^1 - \upsilon^a)\ \text{GPa} \qquad 4.20$$

$$\sigma^1 = 0.084(\upsilon^1 - \upsilon^a) - 2.8644\ \text{GPa} \qquad 4.21$$

$$\sigma^1 = 0.036(\upsilon^1 - \upsilon^a) + 1.1697\times 10^{-5} \times(\upsilon 1 - \upsilon a)^2 + 0.93\ \text{GPa} \qquad 4.22$$

Eq. 4. 23, Eq.4. 24, and Eq.4. 25 represent regions 1,2 and 3 of the left-propagating wave respectively in steel.

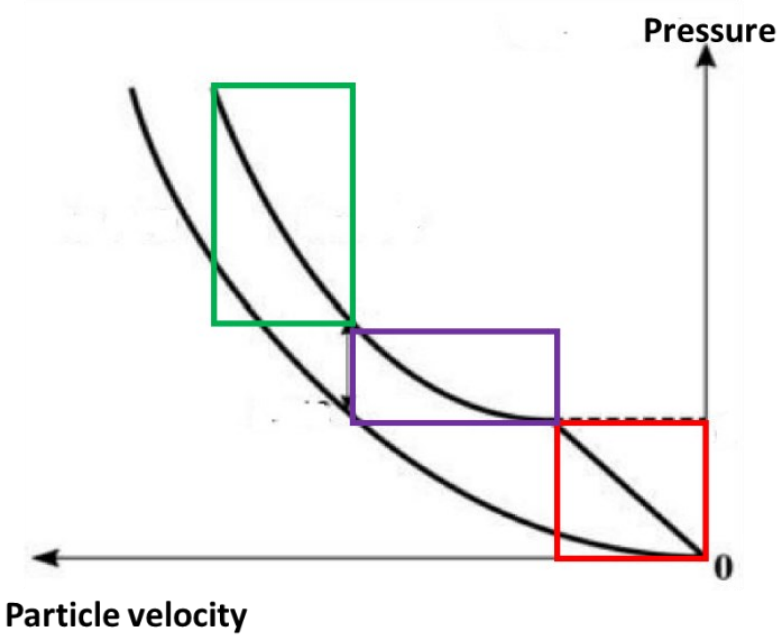

Figure 4.10 Modified P-V Hugoniot curve for left-going shock wave

$$\sigma^1 = -0.041(\upsilon^1 - \upsilon^a)\ \text{GPa} \quad 4.23$$

$$\sigma^1 = -0.084(\upsilon^1 - \upsilon^a) - 2.8644\ \text{GPa} \quad 4.24$$

$$\sigma^1 = -0.036(\upsilon^1 - \upsilon^a) + 1.1697\times 10^{-5} \times(\upsilon 1 - \upsilon a)^2 + 0.93\ \text{GPa} \quad 4.25$$

4.5 Development of the Algorithm

The developed algorithms for elastic wave propagation and shock wave propagation are almost similar and only the wave interaction solving approach varies from one to another.

The developed algorithm tracks each wave and stores the corresponding stress, particle velocity, the material wherein the wave is traveling, wave propagating velocity and direction, and the starting and ending points of each wave. Then the program identifies the possible wave-wave, wave-interface, and wave-boundary interactions and chooses the interaction that occurs at the earliest time. Then the algorithm solves the selected interaction and adds newly generated waves to the system while removing the interacted waves. After each interaction, the state parameters are updated. Likewise, the algorithm repeats until all the possible interactions are solved or until the given number of loops are completed.

When a tensile stress is generated at an interface due to a wave-interface interaction, two materials get separated as the bonding stress of the interface is zero which results in two additional free surfaces in the system. Then, the main algorithm is not valid anymore. To address this specific scenario, several sub-algorithms were developed in each test case. When the program identifies a separation at an interface, it automatically terminates the main algorithm and executes the corresponding sub-algorithm. For example, 7 different algorithms (main algorithm and 6 sub-algorithms) were developed for the tri-metallic steel-titanium-aluminium test case as there are totally 3 different material interfaces.

The summary of the developed algorithms for both elastic and shock wave propagation is described in the following flowchart. Only the 'Solving Interactions' step varies from one to another.

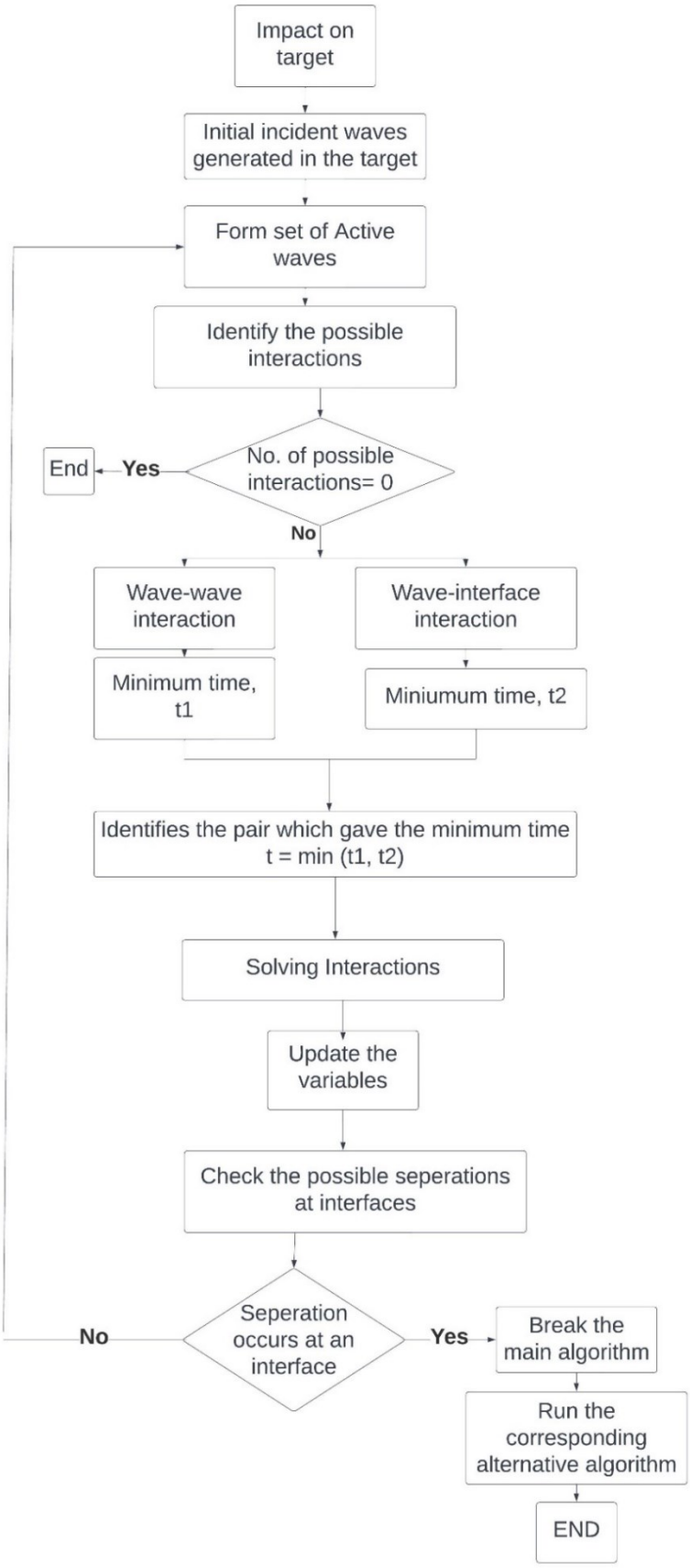

Figure 4.11 Summary of the developed algorithm

5 RESULTS AND DISCUSSION

The outcomes from the numerical and analytical models for both elastic and shock wave propagation are presented and discussed in the following sub-sections.

5.1 Numerical Model Validation

As it was mentioned earlier, the study consists of two major components. 1) Elastic wave propagation and 2) Shock wave propagation. The method followed to develop the numerical models for both components was the same and only the flyer velocities varied (180 ms^{-1} and 350 ms^{-1} for elastic and shock wave studies respectively). In both cases, the free surface velocity history profiles of the last material of the target obtained from the numerical models were compared with available experimental results.

5.1.1 Experimental results

The experimental results for elastic wave propagation were extracted from a previously done study [40] using a single-stage gas gun test. During the tests, a VMS-2000B Velocimeter was used to measure the flyer velocity, and a PDV to record the velocity history profiles at the target's back-free surface.

Figure 5.1 Single-stage gas gun

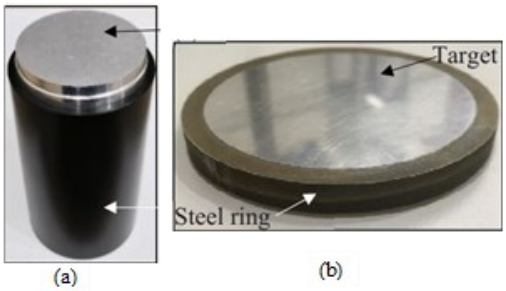

Figure 5.2 (a) Metallic flyer (b) Multi-metallic target

The experimental results for shock wave propagation were also extracted by a similar study [43]. The metallic target was kept inside a steel ring which can be considered as a radially fixed condition. The flyer was also fixed to a sabot.

5.1.2 Validation of Numerical Model for Elastic Wave Propagation

The free surface velocity history profiles of the last material of the target obtained from the numerical models were compared with the aforementioned experimental results. Bi-metallic steel-aluminium (SA) and tri-metallic steel-titanium-aluminium (STA) test cases were considered for the validation process.

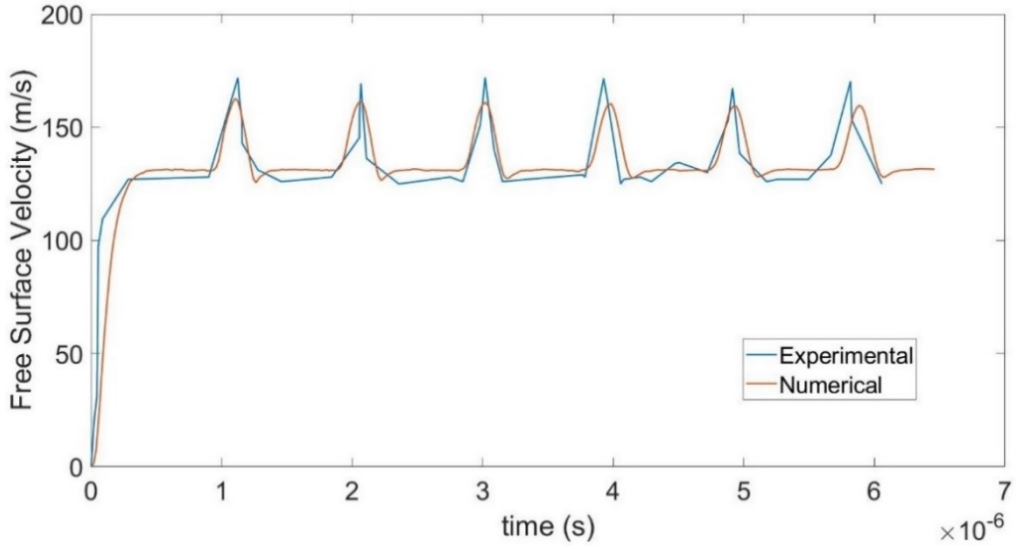

Figure 5.3 Free surface velocity histories comparison for SA

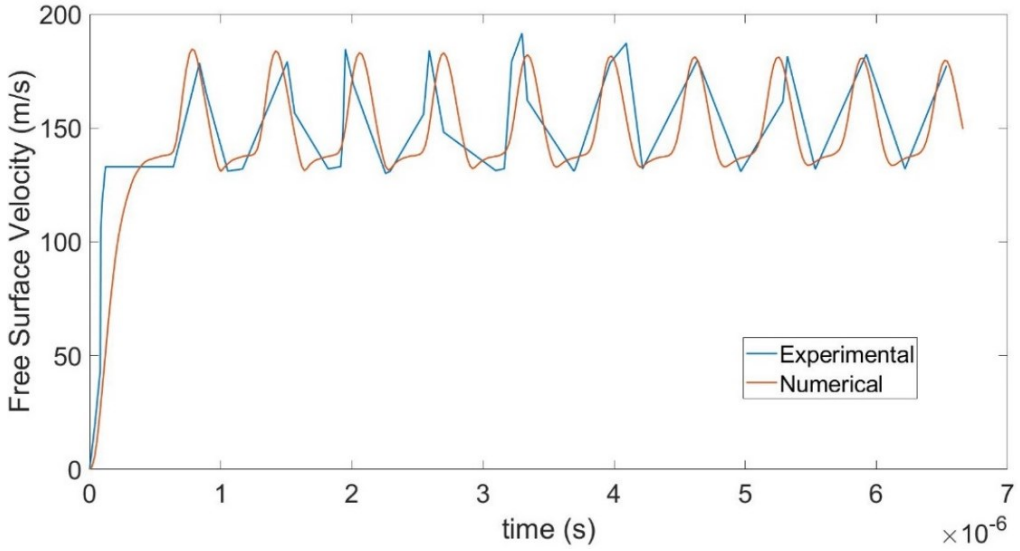

Figure 5.4 Free surface velocity histories comparison for STA

It can be identified that the results obtained from the numerical models are well consistent with the experimental results. However, some minor variations in stress magnitudes and corresponding time can be identified. Also, the tri-metallic steel-titanium-aluminium (STA) test case consists of more oscillations compared to the bi-metallic (SA) one because of its less thickness.

Even though an initial flyer velocity of 180 ms^{-1} was selected for the elastic wave propagation test cases, in the experiment, the velocities of the aluminium flyer just before the impact were slightly varied. It has been mentioned a velocity of 173 ms^{-1} for the SA bi-metallic test case and 171 ms^{-1} for the STA tri-metallic test case. So, those flyer velocities were incorporated into the numerical models to purely match the experiments.

When the stress magnitudes corresponding to peaks were compared, it was identified that the experimental results exceeded the numerical results by 5-7% for the steel-aluminium (SA) bi-metallic test case. However, in the steel-titanium-aluminium (STA) tri-metallic test case the difference between stress magnitudes corresponding to peaks has been reduced up to 3-5%. Also, the numerical model shows a smooth variation while the experiment results show an arbitrary variation. This could be mainly due to the effect of the steel ring in which the target was kept. Even though the perimeter of the target was assumed to be a free surface, it was in touch with the ring which affected the transmission and reflection of waves. Also, the variation of material properties throughout the metallic plates could be attributed to these variations. Even though, these materials are expected to be homogeneous, in the real scenario they consist of some heterogeneity.

Another significant reason for the mismatch in stress values would be the wave propagation velocity values used in the numerical models. The wave speeds used in the numerical models (in GRUNEISEN_EOS) were extracted from the previous studies. However, the materials used in the experiments might have different wave speeds. Therefore, minor variations in both stress magnitude and corresponding time can be identified. However, since only minor deviations were identified, the developed numerical model simulates the elastic wave propagation within multi-metallic systems to an acceptable level.

In the experiment, the metallic plates were kept in a metallic ring as shown in Fig. 5.2 (b). The connection between the target and the ring is neither fully fixed nor free. Therefore, another numerical model was developed allowing translations along the X direction which resulted in following free surface velocity history profiles.

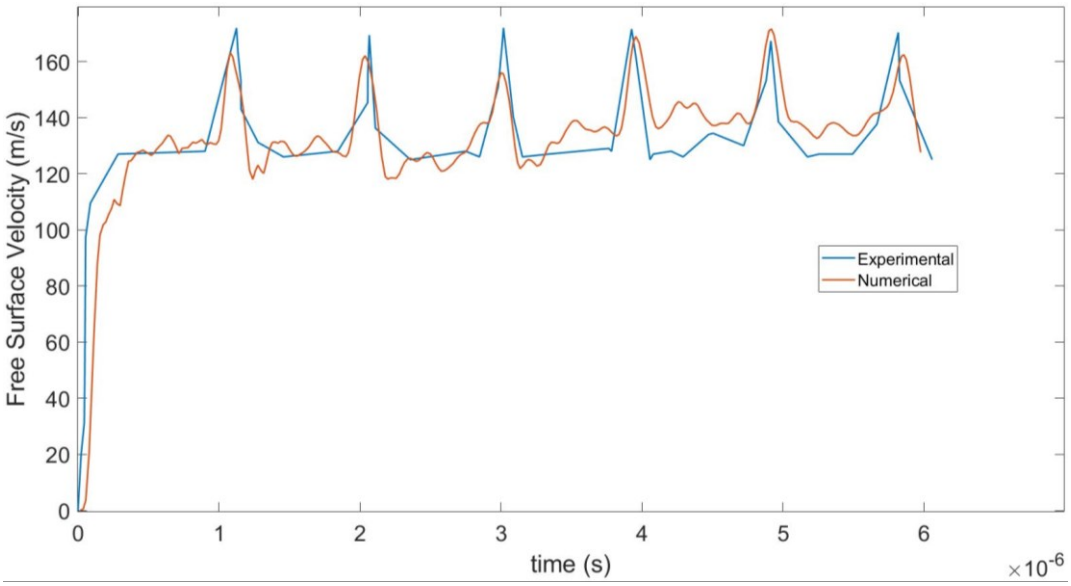

Figure 5.5 Free surface velocity histories comparison for SA without constraints on X direction

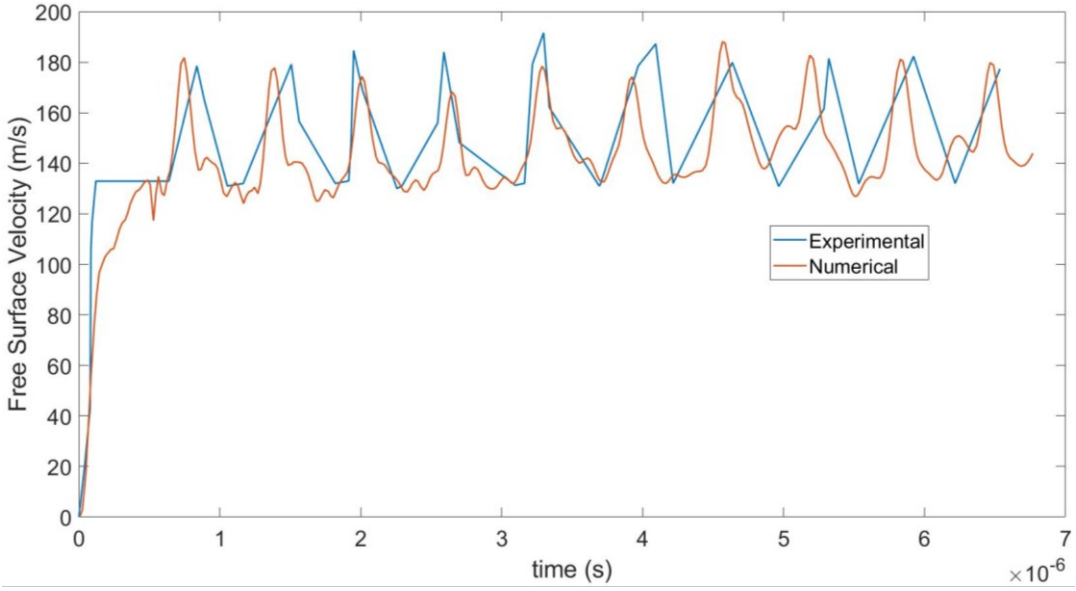

Figure 5.6 Free surface velocity histories comparison for STA without constraints on X direction

It can be identified that the previous model (with translational constraints along the

X direction) is more consistent with the experimental results compared to the latter one (without translational constraints along the X direction) in terms of variation pattern and peak velocity magnitudes. Therefore, from here onwards, the model with translational constraints was used to validate the analytical models.

5.1.3 Validation of Numerical Model for Shock Wave Propagation

For shock wave propagation, only the steel-steel monolithic test case was considered and the same procedure was followed to validate the numerical model.

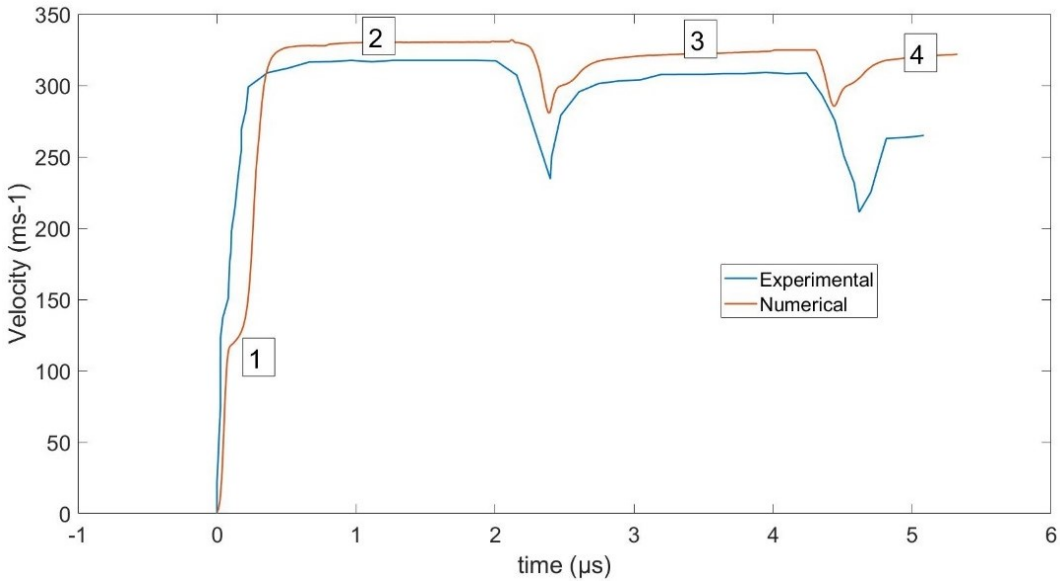

Figure 5.7 Free surface velocity histories comparison for steel monolithic target

It can be identified that the mismatch between the two curves increases with time. The numerical results exceeded the experimental results by 4.38% at the beginning and 17.44% at the end.

The particle velocity that occured due to the initial elastic wave is denoted by point (1) and its magnitude is equal to two times the particle velocity at which the Hugoniot Elastic Limit (HEL) is reached. The plateau (2) corresponds to the particle velocity of the right-going shock wave, which is generated after the wave-wave interaction between the initial shock wave and the reflected elastic wave at the free surface. The left-going shock wave interacts with the flyer-target interface and generates a tensile stress which causes the separation. The plateau (3) occurs after the separation of the flyer and target. After the separation, both faces of the steel

target become free surfaces. The plateau (3) and (4) also correspond to the particle velocities corresponding to the right-going stress wave generated after the wave-wave interaction between the two remaining waves in the steel target. Due to the dissipation of energy occurring during the wave propagation, wave-wave, and wave-free surface interaction, the free surface velocity decreases over time.

5.2 Analytical Model Validation

5.2.1 Analytical Model for Elastic Wave Propagation

The analytical model was validated by comparing the stress-time histories against the results obtained from the already validated numerical model. The stress vs. time variation of an element at the center of the last material was considered for each test case as shown in Fig. 5.6.

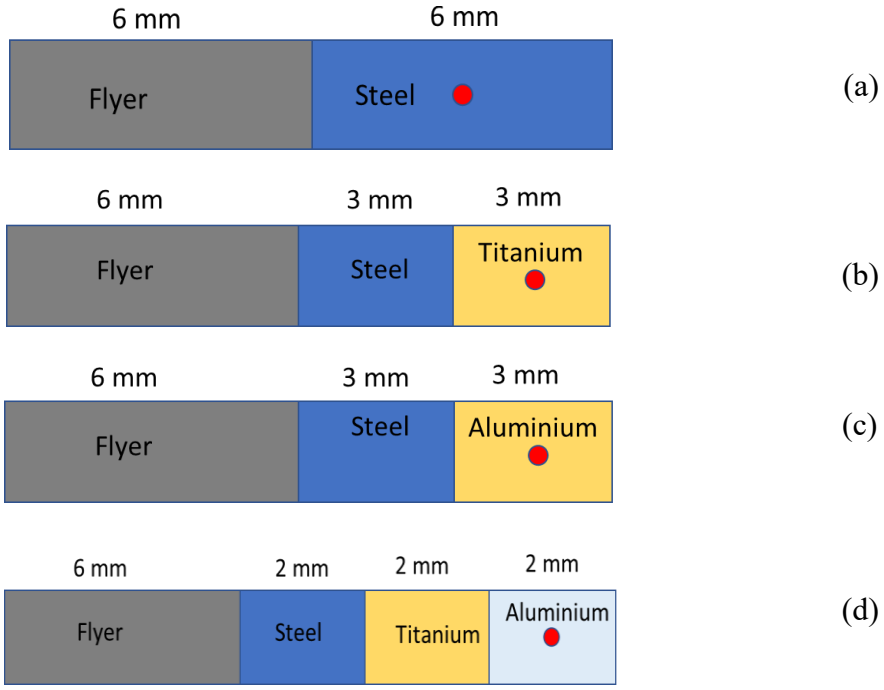

Figure 5.8 Selected element at the center of the last material (a) S (b) ST (c) SA (d) STA

5.2.1.1 Monolithic Steel (S) Test Case

Fig 5.7 shows the stress vs. time variation obtained from numerical and analytical models for monolithic steel (S). The initial peak stress obtained by the analytical model exceeds that of the numerical model by 6.5%. It is shown that the outputs from the numerical model agree well with that of the analytical model in the remaining part.

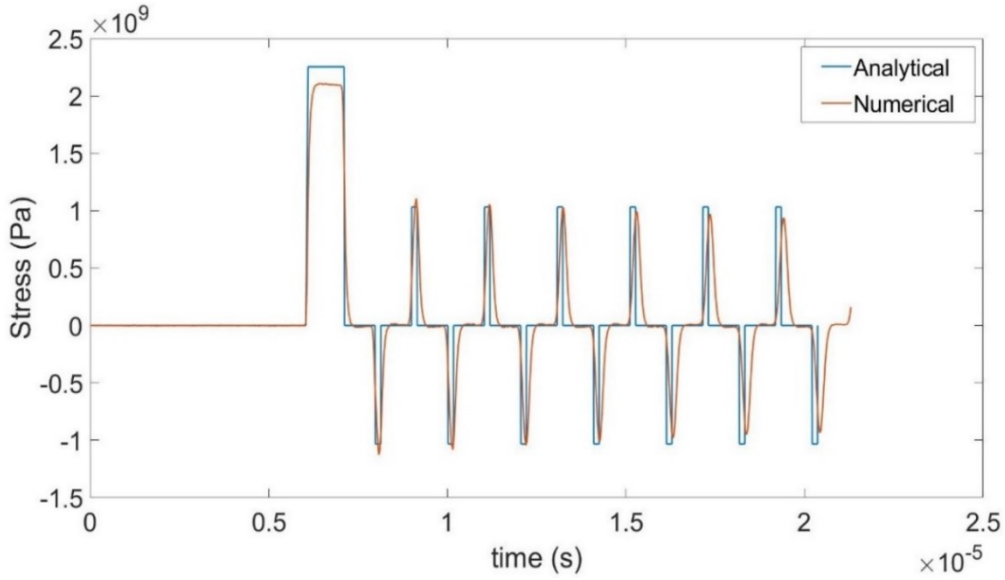

Figure 5.9 Stress vs time variation for monolithic steel (S) test case

5.2.1.2 Bi-metallic Steel-Aluminium (SA) Test Case

Fig 5.8 shows the stress vs. time variation obtained from numerical and analytical models for the bi-metallic steel-aluminium (SA) test case. Even though the initial peak stress values obtained from both models are almost the same, in the remaining section, minor differences can be identified in the variation pattern between the two outputs. The numerical output consists of some additional minor stress peaks compared to that of the analytical model which needs to be studied further.

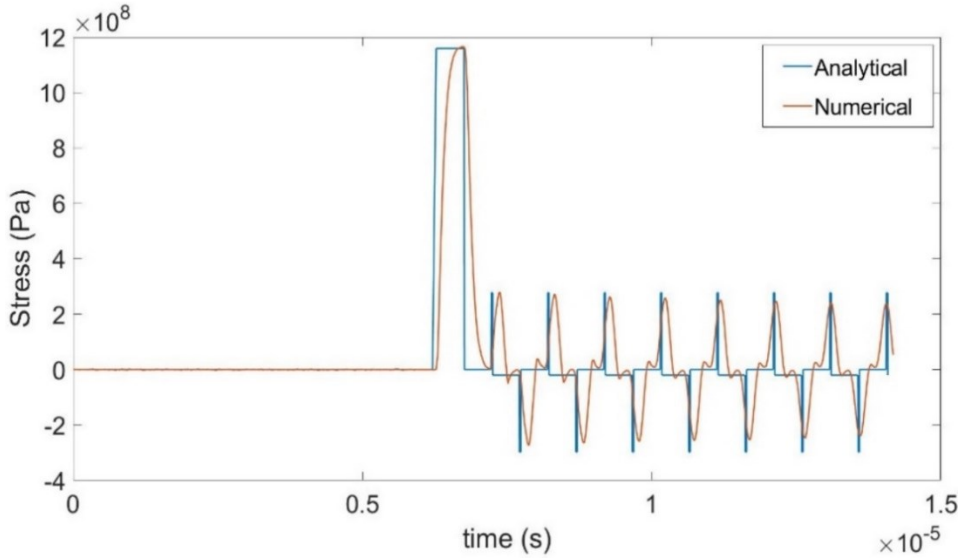

Figure 5.10 Stress vs time variation for bi-metallic steel-aluminium (SA) test case

5.2.1.3 Bi-metallic Steel-Titanium (ST) Test Case

Fig 5.9 shows the stress vs. time variation obtained from numerical and analytical models for the bi-metallic steel-titanium (ST) test case. The peak stress values obtained from both models agree well with each other with a maximum difference of 22%. However, the difference between the two outputs increases with the time.

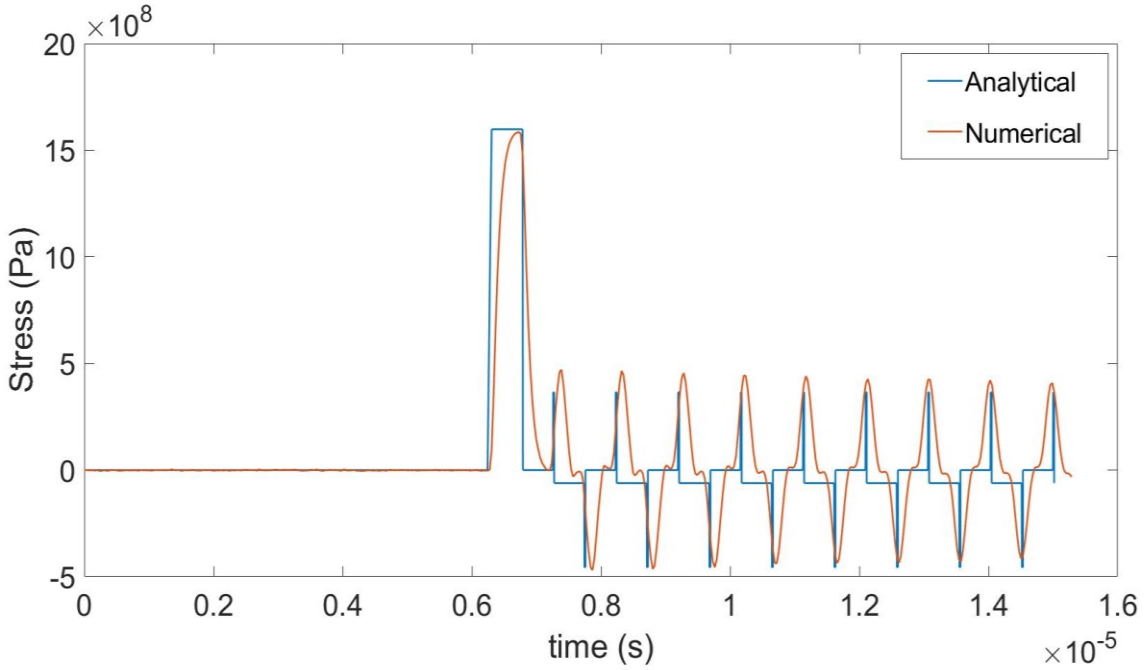

Figure 5.11 Stress vs time variation for bi-metallic steel-titanium (ST) test case

5.2.1.4 Tri-metallic Steel-Titanium-Aluminium (STA) Test Case

Fig 5.10 shows the stress vs. time variation obtained from numerical and analytical models for the tri-metallic steel-titanium-aluminium (STA) test case. The difference between the two outputs corresponding to the initial peak is as high as 9.3%. Also, a significant difference can be identified in the remaining part.

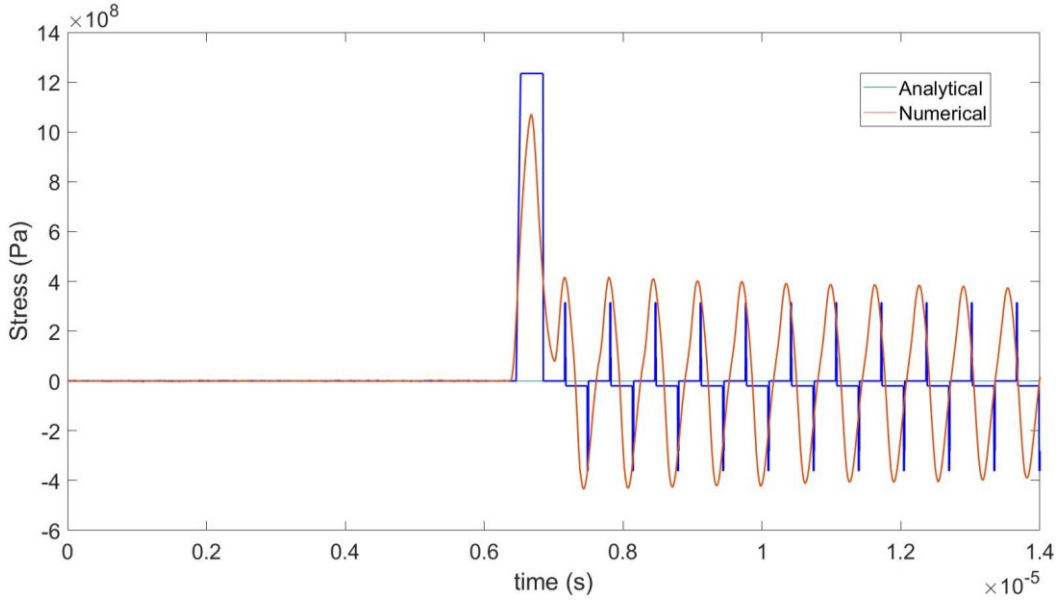

Figure 5.12 Stress vs time variation for tri-metallic steel-titanium-aluminium (STA) test case

The stress wave structure reveals the main difference between the results of analytical and numerical models. In the analytical study, stress waves are idealized as a discontinuity that does not define the intermediate stresses but only the starting and ending stresses. However, in the real scenario, it consists of a structure where the state of stress changes instantly but smoothly across a region to connect the starting and ending stresses. Time-dependent inelastic processes such as viscoelasticity, viscoplasticity, and twinning cause to generate that specific shaped wave structure [7].

Also, the developed analytical model is incapable of finding the wave rise time. As a result, the exact time interval in which the peak stress remains cannot be found by the analytical model.

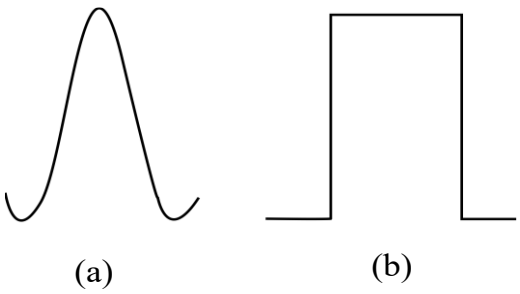

Figure 5.13 Stress wave structures (a) numerical model (b) analytical model

Also, stress peaks are shifted with time in all four cases. This is mainly due to the decrease of the wave rise time along the time axis in the numerical output. Due to the dissipation of the energy, the peak stresses of the numerical output decrease over time. As a result, the corresponding wave rise time also decreases simultaneously. Therefore, with time, stress peaks in the numerical output are shifted slightly. Another reason would be differences in elastic wave propagation velocities used in the analytical and numerical models. In the numerical model, bulk wave speed (CB) was considered which was converted into longitudinal wave speed by the software itself. However, in the analytical model, the theoretically derived longitudinal wave speeds were considered that could be different from those wave speeds used in the numerical models.

Also, some minor variations can be identified in the magnitude of peak stresses. The maximum stress magnitude difference was identified at the first peak of the tri-metallic test case and it is 9.3%. The other variations are in between 3-8%. Also, in the outputs obtained from the numerical model, it is shown that the magnitude of the peak stresses decreases with time because of the dissipation of energy. However, in the analytical results, the peak stresses remain constant over time as shown in Fig. 5.12.

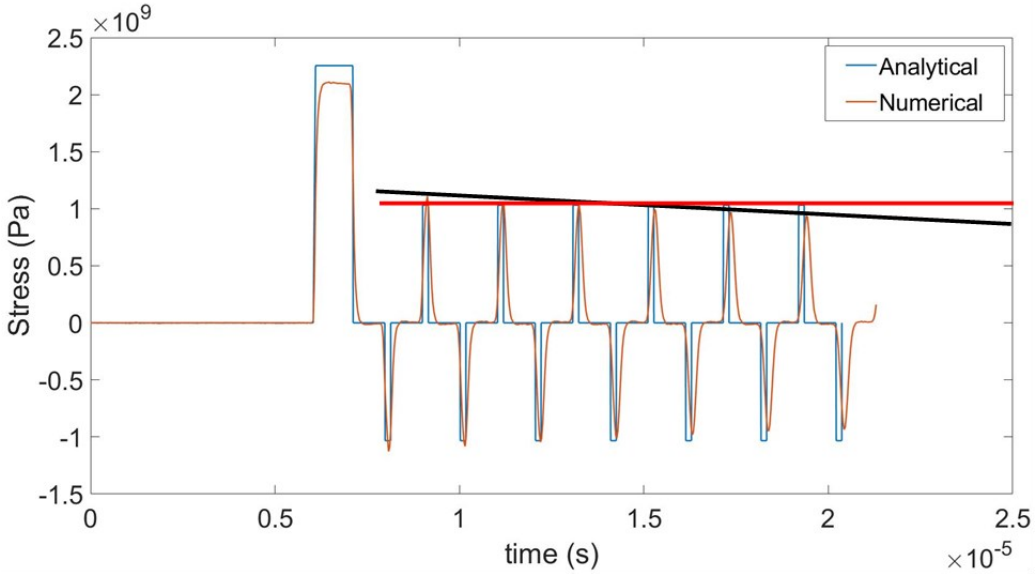

Figure 5.14 Comparison of Energy dissipation output between analytical and numerical models

This is mainly due to the isothermal assumption that was considered in deriving analytical solutions. The energy conservation theorem suggests that the rate of energy increase within the system is balanced by four components; (1) Energy provided by forces acting on the surface (2) Heat transferred out of the system (3) External forces applied within the the volume of the body, and (4) Heat transferred into the system [31]. However, under the isothermal assumption, the temperature in the system is constant and the thermal equilibrium is maintained because the system's heat transmission occurs so slowly. Therefore, the dissipation of the energy during the wave propagation, which results in a reduction in both specific strain energy and specific kinetic energy cannot be simulated analytically.

Also, the fundamental energy balance equation does not address the energy dissipation that occurred during the wave-wave interaction and wave-interface interaction. Because of these two major drawbacks, the analytically obtained peak stresses remain constant over time. Consequently, the accuracy of the stress-time variation given by the analytical model reduces with time.

One of the major findings of this study is that there might be shock waves generated inside the target materials due to the elastic wave-wave interactions. In previous studies, it has been concluded that there will not be shock waves generated inside the target system if the initial incident stress wave that was generated in the first target material is lower than its' HEL. However, it was found that there might be shock waves generated inside the target materials due to the wave-wave interactions even though both waves are elastic waves. It can be simply proved as follows.

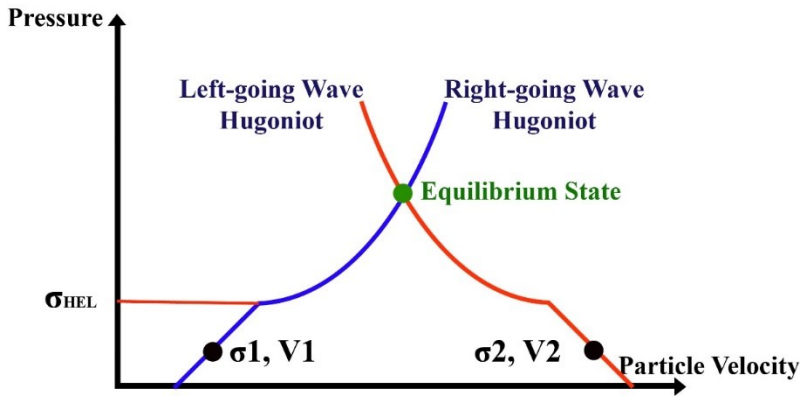

Figure 5.15 Generation of shock waves due to elastic wave-wave interaction

When two elastic waves interact with each other whose particle velocities are far away from each other, the intersecting point of the two Hugoniots (equilibrium state) would be above the HEL value, as shown above, which results in a shock wave.

5.2.2 Analytical Model for Shock Wave Propagation

To validate the developed analytical model, only a steel monolithic test case was considered. The stress vs. time variation of an element at the center of the steel target was considered for the validation as shown in Fig. 5.8 (a).

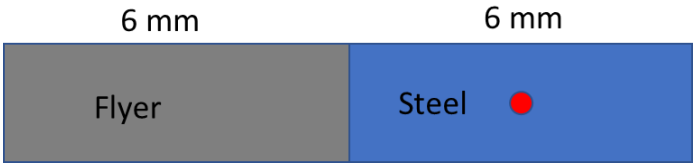

Figure 5.8 (a) Selected element at the center of the last material

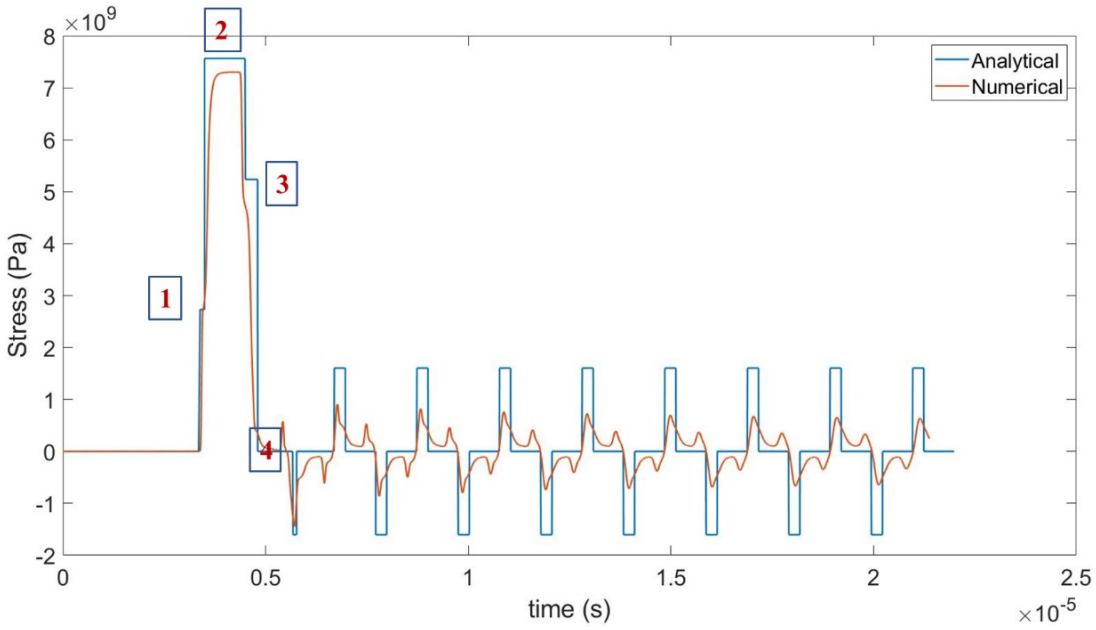

Figure 5.16 Stress vs time variation

The small plateau denoted by (1) is due to the foregoing elastic wave before the initial shock wave whose magnitude is equal to the HEL limit of the material. The plateau (2) represents the arrival of the incident shock wave. Then the right-going shock wave and left-going reflected elastic wave interact with each other and result in two newly generated waves. Those waves take the entire material into a stress

state of 5.23 GPa as shown by the plateau (3). Then the left-going wave interacts with the material interface and generates a tensile stress which causes the separation of the target and the impactor which is shown by point (4).

It is shown that, even though the analytical model is capable of predicting the stress vs. time variation before the separation of the target and impactor, it does not predict the response accurately after the separation. A significant variation can be identified in both the peak stress magnitude and the variation pattern.

Just after the separation, both the left side surface of the target and the right side surface of the flyer become free surfaces. The stress generated at the interface which caused the separation is about 5.17 GPa. However, with the separation, the stress at the free surfaces becomes 0 GPa immediately. Accordingly, the corresponding particle velocity also varies along the Hugoniot. This scenario can be graphically represented as shown below.

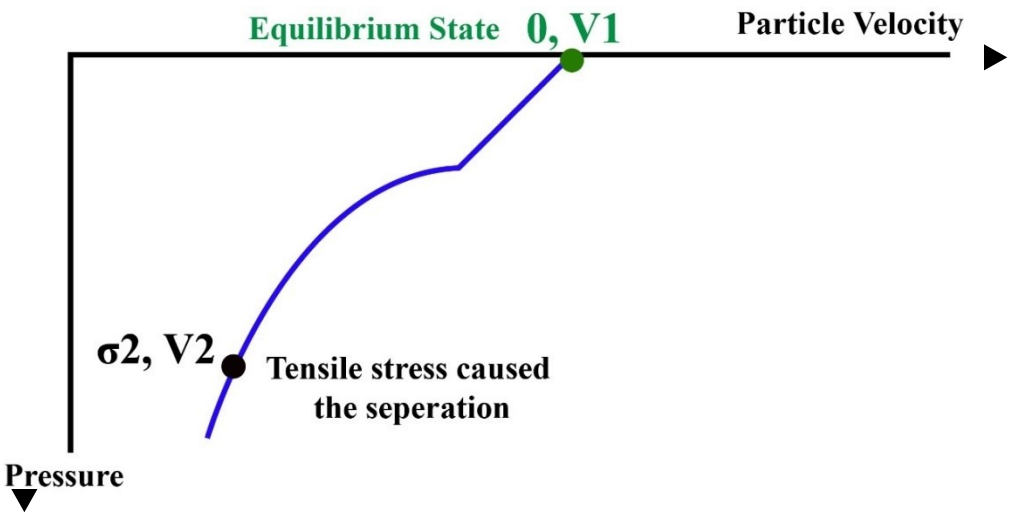

Figure 5.17 Graphical representation of the separation of flyer and target

Even though this concept is theoretically accurate, it does not fully represent the actual behavior at the separation. As a result, the following stress peaks deviate slightly from the numerical outputs. Therefore, an alternative approach should be developed to predict the particle velocity at the free surface just after the separation.

Even in this model, an isothermal condition was assumed. So, it does not give any sense about the amount of energy dissipated during shock propagation and interaction.

6 CONCLUSION

A research study on developing a numerical and analytical model to predict the elastic and shock wave propagation through a multi-metallic system subjected to high-velocity impact loads has been presented in this dissertation. It consists of two major parts. (1) Development of a numerical and analytical model for elastic wave propagation and (2) Development of a numerical and analytical model for shock wave propagation. The developed numerical models were validated against the existing experimental results and those validated numerical models were used to verify the analytical models. The major accomplishments and problems are summarised here and future research directions are presented.

6.1 Important Findings and Discussion

One of the major findings of this study is that there might be shock waves generated inside the target materials due to the elastic wave-wave interactions. It was thoroughly explained in Section 5.

The governing equations employed in both analytical models (elastic and shock) have been derived based on the 1D wave propagation. They do not address the effect of transverse/ radial waves which get reflected at the perimeter and propagate back into the target system. But in the real scenario, the longitudinal waves get affected and degraded with time by the radial waves which cannot be tracked analytically. Therefore, the stress vs. time variations obtained from the analytical model would be accurate only for a limited period (until the effect of transverse waves is negligible).

The experimentally obtained free surface velocity history profiles corresponding to elastic wave propagation show an arbitrary behavior with some abrupt changes in stress-time variation as opposed to the smoothly varied profiles obtained from the numerical models. These slight differences occur mainly due to the material's heterogeneity. Even though the metallic plates used in the experiment were considered to be homogeneous, their material properties vary throughout the target materials. However, those minor variations in the material properties cannot be incorporated into the numerical model.

It is worth mentioning that in both cases, the numerical models are capable of

simulating the free surface velocity variation with reasonable accuracy. In terms of elastic wave propagation, the difference between experimental and numerical outputs varies between 3-7% where it increases up to 4.38-17.44% when it comes to shock wave propagation. So, the idealization of the 3D numerical model into a 2D model can be justified.

The developed analytical model for elastic wave propagation is capable of predicting the stress time histories with a variation of 3-10% when compared to the numerical outputs. Hence, it indicates that the developed algorithm is capable of identifying the correct wave interaction and associated Reimann problem, and then solving it accurately. However, the developed analytical model for shock wave propagation provides accurate results only up to the separation. A significant variation can be identified in both the peak stress magnitude and the variation pattern after the separation of the target and the flyer. This is mainly due to the incapability of the developed analytical model to find the particle velocity at the free surface just after the separation.

Also, the developed analytical models for both cases are incapable of predicting the amount of energy dissipated during stress wave propagation and wave interaction due to the assumption of isothermal behavior. Therefore, the accuracy of the magnitude of peak stresses given by the analytical models reduces with time.

Even though the analytical model consists of some drawbacks as discussed above, it can be used to obtain some crucial outputs that cannot be obtained from finite element analysis (FEA). The debonding stress or the required bonding stress to avoid debonding at material interfaces is the most important thing that is tedious to find from an FEA. It can be easily found with the corresponding time of separation using the analytical model. Also, the analytical model tracks each interaction with the corresponding time which is almost impossible to do in an FEA. As well as the algorithm stores the attributes of each wave including starting point, ending point, travel time, wave speed and direction, corresponding particle velocity, and stress and strain generated after the wave. Further, every FEA model has limited resolution even if the mesh is extremely fine. So, it might be an issue in this kind of study where a stress wave has multiple interactions and reflections. The analytical model is efficient compared to the numerical model in terms of required computational

power. So, the analytical model can be found as a more effective alternative, which can be used for future studies involving multi-metallic target systems.

6.2 Recommendation for Future Works

One of the major drawbacks of the developed analytical models in this study is that they do not give any sense of the amount of energy dissipated during stress wave propagation and interaction. So, the amount of heat transferred into or out of the system can be considered in future studies for better accuracy of results.

Also, the energy dissipation that occurs when a wave interacts with a material interface or with another wave is not described by the aforementioned energy balance theorem. It only gives the amount of energy dissipated during the wave propagation. So, an alternative energy balance theorem can be developed to account for the energy dissipation during wave interactions.

In this study, the development of the wave structure was neglected. Instead of that a discontinuous wave pulse was incorporated. Therefore, it does not give an idea about the wave rise time and the actual time interval in which peak stress remains. So, a detailed study can be carried out to find the development of smooth continuous wave pulses during wave propagation.

The variation of particle velocity at the free surface just after the separation is not fully captured by the proposed model. So, an alternative approach can be considered to predict it.

Also, no higher dimension wave propagation or oblique impacts can be captured by the proposed analytical model. It is only valid for a symmetric one-dimensional plane wave propagation. So, future work could involve the extension of the current study for oblique impacts and higher-dimension wave propagation.

Also, in this study, the comparison between analytical and numerical models was limited to only the stress-time variation. However, energy is one of the main parameters that should be taken into account in the comparisons that can be considered in future works.

7 REFERENCES

[1] S. P. Singh, H. Singh, and P. Mahajan, “A generalized model for one-dimensional impact response of a heterogeneous layered medium,” *International Journal of Impact Engineering*, vol. 173, p. 104433, Mar. 2023, doi: 10.1016/j.ijimpeng.2022.104433.

[2] Q. M. Li, S. R. Reid, H. M. Wen, and A. R. Telford, “Local impact effects of hard missiles on concrete targets,” *International Journal of Impact Engineering*, vol. 32, no. 1–4, pp. 224–284, Dec. 2005, doi: 10.1016/j.ijimpeng.2005.04.005.

[3] S. Nikbakht, S. Kamarian, and M. Shakeri, “A review on optimization of composite structures Part II: Functionally graded materials,” *Composite Structures*, vol. 214, pp. 83–102, Apr. 2019, doi: 10.1016/j.compstruct.2019.01.105.

[4] M. A. Meyers, *Dynamic behavior of materials*. New York: Wiley, 1994.

[5] J. A. Zukas, *Introduction to hydrocodes*. in Studies in applied mechanics, no. 49. Amsterdam: Elsevier, 2004.

[6] X. Chen, N. Chandra, and A. M. Rajendran, “Analytical solution to the plate impact problem of layered heterogeneous material systems,” *International Journal of Solids and Structures*, vol. 41, no. 16–17, pp. 4635–4659, Aug. 2004, doi: 10.1016/j.ijsolstr.2004.02.064.

[7] V. Agrawal and K. Bhattacharya, “Shock wave propagation through a model one dimensional heterogeneous medium,” *International Journal of Solids and Structures*, vol. 51, no. 21–22, pp. 3604–3618, Oct. 2014, doi: 10.1016/j.ijsolstr.2014.06.021.

[8] G. A. Gazonas, A. P. Velo, and R. A. Wildman, “Asymptotic impact behavior of Goupillaud-type layered elastic media,” *International Journal of Solids and Structures*, vol. 96, pp. 38–47, Oct. 2016, doi: 10.1016/j.ijsolstr.2016.06.024.

[9] S. Astarlioglu and T. Krauthammer, “Response of normal-strength and ultra-high-performance fiber-reinforced concrete columns to idealized blast loads,” *Engineering Structures*, vol. 61, pp. 1–12, Mar. 2014, doi: 10.1016/j.engstruct.2014.01.015.

[10] C. Zhang, G. Gholipour, and A. A. Mousavi, “Blast loads induced responses of RC structural members: State-of-the-art review,” *Composites Part B: Engineering*, vol. 195, p. 108066, Aug. 2020, doi: 10.1016/j.compositesb.2020.108066.

[11] E. J. Conrath, Structural Engineering Institute, and American Society of Civil Engineers, Eds., *Structural design for physical security: state of the practice*. Reston, Va: SEI : ASCE, 1999.

[12] A.-H. I. Mourad, A. H. Idrisi, N. Zaaroura, M. M. Sherif, and H. Fouad, “Damage assessment of nanofiller-reinforced woven kevlar KM2plus/Epoxy resin laminated composites,” *Polymer Testing*, vol. 86, p. 106501, Jun. 2020, doi: 10.1016/j.polymertesting.2020.106501.

[13] M. A. Caminero, I. García-Moreno, and G. P. Rodríguez, “Damage resistance of carbon fibre reinforced epoxy laminates subjected to low velocity impact: Effects of laminate thickness and ply-stacking sequence,” *Polymer Testing*, vol. 63, pp. 530–541, Oct. 2017, doi: 10.1016/j.polymertesting.2017.09.016.

[14] J. Leijten, H. E. N. Bersee, O. K. Bergsma, and A. Beukers, “Experimental study of the low-velocity impact behaviour of primary sandwich structures in aircraft,” *Composites Part A: Applied Science and Manufacturing*, vol. 40, no. 2, pp. 164–175, Feb. 2009, doi: 10.1016/j.compositesa.2008.10.019.

[15] C. Fallon and G. J. McShane, “Impact damage protection mechanisms for elastomer-coated concrete,” *International Journal of Protective Structures*, vol. 12, no. 3, pp. 377–395, Sep. 2021, doi: 10.1177/2041419620984811.

[16] A. M. Remennikov, S. Y. Kong, and B. Uy, “The response of axially restrained non-composite steel–concrete–steel sandwich panels due to large impact loading,” *Engineering Structures*, vol. 49, pp. 806–818, Apr. 2013, doi: 10.1016/j.engstruct.2012.11.014.

[17] R. P. Bohara, S. Linforth, T. Nguyen, A. Ghazlan, and T. Ngo, “Anti-blast and -impact performances of auxetic structures: A review of structures, materials, methods, and fabrications,” *Engineering Structures*, vol. 276, p. 115377, Feb. 2023, doi: 10.1016/j.engstruct.2022.115377.

[18] N. S. Ha and G. Lu, “A review of recent research on bio-inspired structures and materials for energy absorption applications,” *Composites Part B: Engineering*, vol. 181, p. 107496, Jan. 2020, doi: 10.1016/j.compositesb.2019.107496.

[19] S. H. Siddique, P. J. Hazell, H. Wang, J. P. Escobedo, and A. A. H. Ameri, “Lessons from nature: 3D

printed bio-inspired porous structures for impact energy absorption – A review," *Additive Manufacturing*, vol. 58, p. 103051, Oct. 2022, doi: 10.1016/j.addma.2022.103051.
[20] Z. Guoqi, W. Goldsmith, and Ck. H. Dharan, "Penetration of laminated Kevlar by projectiles—I. Experimental investigation," *International Journal of Solids and Structures*, vol. 29, no. 4, pp. 399–420, 1992, doi: 10.1016/0020-7683(92)90207-A.
[21] S. K. Roy, M. Trabia, B. O'Toole, and M. Pena, "Study of Hypervelocity Projectile Impact on Thick Metal Plates," *Shock and Vibration*, vol. 2016, pp. 1–11, 2016, doi: 10.1155/2016/4313480.
[22] F. J. Zerilli and R. W. Armstrong, "Dislocation-mechanics-based constitutive relations for material dynamics calculations," *Journal of Applied Physics*, vol. 61, no. 5, pp. 1816–1825, Mar. 1987, doi: 10.1063/1.338024.
[23] Y. Cao, H. S. Di, R. D. K. Misra, and J. Zhang, "Hot Deformation Behavior of Alloy 800H at Intermediate Temperatures: Constitutive Models and Microstructure Analysis," *J. of Materi Eng and Perform*, vol. 23, no. 12, pp. 4298–4308, Dec. 2014, doi: 10.1007/s11665-014-1220-4.
[24] V. Kumar, V. Yadav, U. Shankar, and G. Suneesh, "A review on Johnson Cook material model," *Materials Today: Proceedings*, vol. 62, pp. 3450–3456, 2022, doi: 10.1016/j.matpr.2022.04.279.
[25] H. Ramírez and C. Rubio-Gonzalez, "Finite-element simulation of wave propagation and dispersion in Hopkinson bar test," *Materials & Design*, vol. 27, no. 1, pp. 36–44, Jan. 2006, doi: 10.1016/j.matdes.2004.08.021.
[26] G. Sun, D. Chen, H. Wang, P. J. Hazell, and Q. Li, "High-velocity impact behaviour of aluminium honeycomb sandwich panels with different structural configurations," *International Journal of Impact Engineering*, vol. 122, pp. 119–136, Dec. 2018, doi: 10.1016/j.ijimpeng.2018.08.007.
[27] R. A. Gingold and J. J. Monaghan, "Smoothed particle hydrodynamics: theory and application to non-spherical stars," *Monthly Notices of the Royal Astronomical Society*, vol. 181, no. 3, pp. 375–389, Dec. 1977, doi: 10.1093/mnras/181.3.375.
[28] W. Yang, R. Ye, P. Ren, and A. Tian, "Antipenetration Performance of Multilayer Protective Structure by the Coupled SPH-FEM Numerical Method," *Shock and Vibration*, vol. 2023, pp. 1–20, Jul. 2023, doi: 10.1155/2023/6225283.
[29] P. L. N. Fernando, D. Mohotti, and A. Remennikov, "An Innovative Approach of Using Continuous Impedance-Graded Metallic Composite System for Attenuation of Stress Waves," *Journal of Applied Mechanics*, vol. 86, no. 6, p. 061002, Jun. 2019, doi: 10.1115/1.4042681.
[30] K. Guo, L. Zhu, Y. Li, and T. X. Yu, "Numerical study on mechanical behavior of foam core sandwich plates under repeated impact loadings," *Composite Structures*, vol. 224, p. 111030, Sep. 2019, doi: 10.1016/j.compstruct.2019.111030.
[31] L. W. Davison, *Fundamentals of shock wave propagation in solids*. in Shock wave and high pressure phenomena. Berlin: Springer, 2008.
[32] J. K. Knowles, "On the relation between particle velocity and shock wave speed for thermoelastic materials," *Shock Waves*, vol. 12, no. 2, pp. 137–144, Aug. 2002, doi: 10.1007/s00193-002-0146-1.
[33] P. W. Cooper, *Explosives engineering*, 1st ed. Weinheim: Wiley-VCH, 2018.
[34] M. Murugesan and D. Jung, "Johnson Cook Material and Failure Model Parameters Estimation of AISI-1045 Medium Carbon Steel for Metal Forming Applications," *Materials*, vol. 12, no. 4, p. 609, Feb. 2019, doi: 10.3390/ma12040609.
[35] E Kelderman, "Mechanical behaviour of armoured steel under high strain rate tensile loading conditions," *The UNSW Canberra at ADFA Journal of Undergraduate Engineering Research, 8(1). (2015)*.
[36] A. E. Buzyurkin, I. L. Gladky, and E. I. Kraus, "Determination and verification of Johnson–Cook model parameters at high-speed deformation of titanium alloys," *Aerospace Science and Technology*, vol. 45, pp. 121–127, Sep. 2015, doi: 10.1016/j.ast.2015.05.001.
[37] A. Manes, M. Pagani, M. Saponara, D. Mombelli, C. Mapelli, and M. Giglio, "Metallographic characterisation of Al6061-T6 aluminium plates subjected to ballistic impact," *Materials Science and Engineering: A*, vol. 608, pp. 207–220, Jul. 2014, doi: 10.1016/j.msea.2014.04.064.
[38] Kasper and Vivian, "Modeling of armour-piercing projectile perforation of thick aluminium plates," presented at the 13th International LS-DYNA Users Conference, 2014. [Online]. Available: https://lsdyna.ansys.com/wp-content/uploads/attachments/modelling-of-armour-piercing-projectile-perforation-of-thick-aluminium-plates.pdf
[39] O. Heuzé, "Complete forms of Mie-Gruneisen equation of state," presented at the SHOCK

COMPRESSION OF CONDENSED MATTER - 2015: Proceedings of the Conference of the American Physical Society Topical Group on Shock Compression of Condensed Matter, Tampa Bay, Florida, USA, 2017, p. 050001. doi: 10.1063/1.4971535.
[40] P. L. N. Fernando, D. Mohotti, A. Remennikov, P. Hazell, H. Wang, and A. Amin, "Stress propagation and debonding effects in impedance-graded multi-metallic systems under impact loading," *International Journal of Protective Structures*, vol. 12, no. 1, pp. 3–21, Mar. 2021, doi: 10.1177/2041419620917709.
[41] S. P. Singh, H. Singh, and P. Mahajan, "Interaction of Shock Waves in a Multi-material System," in *Recent Advances in Applied Mechanics*, T. Tadepalli and V. Narayanamurthy, Eds., in Lecture Notes in Mechanical Engineering. , Singapore: Springer Singapore, 2022, pp. 547–559. doi: 10.1007/978-981-16-9539-1_40.
[42] P. J. Hazell, *Armour: materials, theory, and design*. Boca Raton, FL: CRC Press, 2016.
[43] P. L. N. Fernando, D. Mohotti, A. Remennikov, P. J. Hazell, H. Wang, and A. Amin, "Experimental, numerical and analytical study on the shock wave propagation through impedance-graded multi-metallic systems," *International Journal of Mechanical Sciences*, vol. 178, p. 105621, Jul. 2020, doi: 10.1016/j.ijmecsci.2020.105621.

8 APPENDICES

8.1 Appendix A: Developed MATLAB code to identify the wave-material interface and wave-wave interaction (Elastic wave propagation – Monolithic Steel (S) test case)

```
%Wave_material_interface interaction
t1 = 10;
II_I =[]; JJ_I = []; tt_I = [];
for i = 1:length(Active)
       for j = 1:3
            if MI(j) ~= X0(i)
                 if MI(j)-X0(i)>0 && C(i)>0 || MI(j)-X0(i)<0 && C(i)<0
                     t = (MI(j)-X0(i))/C(i);
                    tt_I = [tt_I, t]; II_I =[II_I, i]; JJ_I = [JJ_I,j];
                    if t < t1
                           t1 = t;
                     end
                end
            end
      end
end
%Check multiple wave-interface interaction at the same time
a = 0;
I_I = []; J_J = [];
for b = 1:length(tt_I)
       if abs(t1 - tt_I(b)) < 1e-12
            a = a+1;
              I_I = [I_I,II_I(b)]; J_J = [J_J,JJ_I(b)];
     end
end
%Wave_wave interaction
t2 = 10;
II_W =[]; JJ_W = []; tt_W = []; R_W = []; C_W = [];
for i = 1:length(Active)
       for j = 1:length(Active)
             if i~=j
                  if (0<= X0(i)) && (X0(i)< X0(j)) && (X0(j)<=0.006) && (C(i)>0 &&
C(j)<0)
                       t = (X0(j)-X0(i))/(C(i)-C(j));
                      II_W =[II_W, i]; JJ_W = [JJ_W, j]; tt_W = [tt_W, t];
                      R_W = [R_W,R_s]; C_W = [C_W, C_s];
                      if t<t2
                            t2 = t;
                      end
                 elseif (-0.006<= X0(i)) && (X0(i)< X0(j)) && (X0(j)<=0) && (C(i)>0 &&
C(j)<0)
                      t = (X0(j)-X0(i))/(C(i)-C(j));
                      II_W =[II_W, i]; JJ_W = [JJ_W, j]; tt_W = [tt_W, t];
                      R_W = [R_W,R_a]; C_W = [C_W, C_a];
                      if t<t2
                         t2 = t;

                      end
                  end
             end
        end
end
%Check multiple wave-wave interaction at the same time
k = 0;
I_W = []; J_W =[];
R_WW = []; C_WW = [];
for b = 1:length(tt_W)
       if abs(t2 - tt_W(b)) < 1e-12
       k = k+1;
            I_W = [I_W,II_W(b)]; J_W = [J_W,JJ_W(b)];
            R_WW = [R_WW, R_W(b)];
```

```
            C_WW = [C_WW, C_W(b)];
        end
end
```

8.2 Appendix B: Developed MATLAB code to solve the elastic wave – material interface/ free surface interaction (Elastic wave propagation – Monolithic Steel (S) test case)

```
elseif t1 < t2 % wave-interface interaction occurs before the wave-wave interaction
    active = []; v = []; x0 = []; t0 = []; c = [];
    for n = 1:a
        I = I_I(n); J = J_J(n);
        Z2_I = Active(I); Z1_I = SI(J); V2_I = V(I); V1_I = VI(J);
        t0_I = T0(I); D0_I = X0(I); D1_I = MI(J); t1_I = t1;
        L =[]; T =[];
        L = [L,[D0_I,D1_I]];
        T = [T,[t0_I,t0_I+t1_I]];
        plot(L,T);

        if C(I)>0 && MI(J)==0
            disp('Positive Wave interacts @ "0" wave-interface');
            %solve linear equations
            V3_Sol = ((R_a*C_a*V2_I)+(R_s*C_s*V1_I)+(Z1_I-Z2_I))/(R_s*C_s + R_a*C_a );
            Z3_Sol = Z2_I + (R_a*C_a)*(V3_Sol-V2_I);

            %Stress History, Velocity History Profiles
            if D0_I <= P && P <= 0
                t_p = t0_I + (P-D0_I)/C(I);
                Z_P = [Z_P, Z2_I]; T_P = [T_P,t_p]; V_P = [V_P, V2_I];
            end
            %Check the tensile stress at interfaces
            if Z3_Sol < 0
                Wa_Se = Z3_Sol;
                L = 1;
                si = SI; vi = VI; si_ = SI; vi_ = VI;
                si_(1) = Z3_Sol; vi_(1) = V3_Sol;
            end

            %Add newly generated waves
            active = [active,Z3_Sol];
            v = [v,V3_Sol];
            x0 = [x0,D1_I];
            t0 = [t0,t0_I+t1_I];
            c = [c,C_s];

            active = [active,Z3_Sol];
            v = [v,V3_Sol];
            x0 = [x0,D1_I];
            t0 = [t0,t0_I+t1_I];
            c = [c,-C_a];

            %update the material interface stress and velocity
            SI(1) = Z3_Sol;
            VI(1) = V3_Sol;

        elseif C(I)<0 && MI(J) == 0
            disp('Negative Wave interacts @ "0" wave-interface');
            %solve linear equations
            V3_Sol = ((R_a*C_a*V1_I)+(R_s*C_s*V2_I)+(Z2_I-Z1_I))/(R_s*C_s + R_a*C_a );
            Z3_Sol = Z1_I + (R_a*C_a)*(V3_Sol-V1_I);

            %Stress History, Velocity History Profiles
            if 0 < P && P <= D0_I
                t_p = t0_I + (P-D0_I)/C(I);
                Z_P = [Z_P, Z2_I]; T_P = [T_P,t_p]; V_P = [V_P, V2_I];
            end
```

```
        %Check the tensile stress at interfaces
        if Z3_Sol < 0
            Wa_Se = Z3_Sol;
            L = 1;
            si = SI; vi = VI; si_ = SI; vi_ = VI;
            si(1) = Z3_Sol; vi(1) = V3_Sol;
        end

        %Add newly generated waves
        active = [active,Z3_Sol];
        v = [v,V3_Sol];
        x0 = [x0,D1_I];
        t0 = [t0,t0_I+t1_I];
        c = [c,-C_a];

        active = [active,Z3_Sol];
        v = [v,V3_Sol];
        x0 = [x0,D1_I];
        t0 = [t0,t0_I+t1_I];
        c = [c,C_s];

        %update the material interface stress and velocity
        SI(1) = Z3_Sol;
        VI(1) = V3_Sol;

    elseif C(I)>0 && MI(J) == 0.006
        disp('Positive Wave interacts @ "0.006 edge" wave-interface');
        Z3_Sol = Z1_I;
        V3_Sol = 2*V2_I - V1_I;

        %Stress History, Velocity History Profiles
        if D0_I <= P && P < 0.006
            t_p = t0_I + (P-D0_I)/C(I);
            Z_P = [Z_P, Z2_I]; T_P = [T_P,t_p]; V_P = [V_P, V2_I];
        end

        %Add newly generated waves
        active = [active,Z3_Sol];
        v = [v,V3_Sol];
        x0 = [x0,D1_I];
        t0 = [t0,t0_I+t1_I];
        c = [c,-C_s];

        %update the material interface stress and velocity
        SI(2) = Z3_Sol;
        VI(2) = V3_Sol;

    elseif C(I)<0 && MI(J) == -0.006
        disp('Negative Wave interacts @ "-0.006 edge" wave-interface');
        Z3_Sol = Z1_I;
        V3_Sol = 2*V2_I - V1_I;

        %Stress History, Velocity History Profiles
        if -0.006 < P && P <= D0_I
            t_p = t0_I + (P-D0_I)/C(I);
            Z_P = [Z_P, Z2_I]; T_P = [T_P,t_p]; V_P = [V_P, V2_I];
        end

        %Add newly generated waves
        active = [active,Z3_Sol];
        v = [v,V3_Sol];
        x0 = [x0,D1_I];
        t0 = [t0,t0_I+t1_I];
        c = [c,C_a];

        %update the material interface stress and velocity
        SI(3) = Z3_Sol;
        VI(3) = V3_Sol;
```

```
        end
    end
```

8.3 Appendix C: Developed MATLAB code to solve the elastic wave – wave interaction (Elastic wave propagation – Monolithic Steel (S) test case)

```
elseif t1>t2 % wave-wave interaction occurs before the wave-interface interaction
    active = []; v = []; x0 = []; t0 = []; c = [];
    for n = 1:k
        I = I_W(n); J = J_W(n); R_W = R_WW(n); C_W = C_WW(n);
        Z2 = Active(J); V2 = V(J); D0_2 = X0(J); t0_2 = T0(J);
        Z1 = Active(I); V1 = V(I); D0_1 = X0(I); t0_1 = T0(I);
        D1 = X0(I) + C_W*t2;

        %Stress History, Velocity History Profiles
        if D0_1 <= P && P <= D1
            t_p = t0_1 + (P-D0_1)/C_W;
            Z_P = [Z_P, Z1]; T_P = [T_P,t_p]; V_P = [V_P, V1];
        elseif D1 <= P && P <= D0_2
            t_p = t0_2 + (P-D0_2)/(-1*C_W);
            Z_P = [Z_P, Z2]; T_P = [T_P,t_p]; V_P = [V_P, V2];
        end

        %Identify the location
        if (-0.006 < D1) && (D1 < 0)
            disp('Wave-wave interaction in Aluminium flyer')
        elseif (0 < D1) && (D1 < 0.006)
            disp('Wave-wave interaction in Steel target')
        end

        % First Wave
        L =[]; T =[];
        L = [L,[D0_1,D1]];
        T = [T,[t0_1,t0_1+t2]];
        plot(L,T);

        %Second wave
        L =[]; T =[];
        L = [L,[D0_2,D1]];
        T = [T,[t0_2,t0_2+t2]];
        plot(L,T);

        %solve linear equations
        V3_Sol = ((R_W*C_W*V1)+(R_W*C_W*V2)+(Z2-Z1))/(R_W*C_W + R_W*C_W);
        Z3_Sol = Z1 + (R_W*C_W)*(V3_Sol-V1);

        %Add newly generated waves
        active = [active,Z3_Sol];
        v = [v,V3_Sol];
        x0 = [x0,D1];
        t0 = [t0,t0_1+t2];
        c = [c,C_W];

        active = [active,Z3_Sol];
        v = [v,V3_Sol];
        x0 = [x0,D1];
        t0 = [t0,t0_2+t2];
        c = [c,-C_W];

    end
```

8.4 Appendix D: Developed MATLAB code to solve the shock wave – material interface interaction (Shock wave propagation – Monolithic Steel (S) test case)

```
active = []; v = []; x0 = []; t0 = []; c = []; stf = [];
for n = 1:a
I = I_I(n); J = J_J(n);
Z2_I = Active(I); Z1_I = SI(J); V2_I = V(I); V1_I = VI(J);
```

```
t0_I = T0(I); D0_I = X0(I); D1_I = MI(J); t1_I = t1;
L =[]; T =[];
L = [L,[D0_I,D1_I]];
T = [T,[t0_I,t0_I+t1_I]];
plot(L,T);

if C(I)>0 && MI(J)==0
    disp('Positive Wave interacts @ "0" wave-interface');
    %solve linear equations
    %Find 'xb' value
    if Z2_I <-ST
        FP1 = [-1.1697e4 -0.036e9 -0.93e9-Z2_I];
        xf2 = roots(FP1); %negative value
        xf = max(xf2(1), xf2(2));
        xb = V2_I - xf;
    elseif (-ST<= Z2_I) && (Z2_I <-HEL)
        FP1 = [0 -0.084e9 2.8644e9-Z2_I];
        xf = roots(FP1); %negative value
        xb = V2_I - xf;
    elseif (-HEL<= Z2_I) && (Z2_I <HEL)
        FP1 = [0 -0.041e9 -Z2_I];
        xf = roots(FP1); %negative value
        xb = V2_I - xf;
    elseif (HEL <= Z2_I) && (Z2_I <= ST)
        FP2 = [0 -0.084e9 -2.8644e9-Z2_I];
        xf = roots(FP2);
        xb = V2_I - xf;
    elseif ST < Z2_I
        FP3 = [1.1697e4 -0.036e9 0.93e9-Z2_I];
        xf2 = roots(FP3);
        xf = min(xf2(1), xf2(2));
        xb = V2_I - xf;
    end

    %Find 'xa' value
    if Z1_I <-ST
        FP3 = [-1.1697e4 0.036e9 -0.93e9-Z1_I];
        xf2 = roots(FP3);
        xf = min(xf2(1), xf2(2));
        xa = V1_I - xf;
    elseif (-ST<= Z1_I) && (Z1_I <-HEL)
        FP1 = [0 0.084e9 2.8644e9-Z1_I];
        xf = roots(FP1); %negative value
        xa = V1_I - xf;
    elseif (-HEL<= Z1_I) && (Z1_I <HEL)
        FP1 = [0 0.041e9 -Z1_I];
        xf = roots(FP1);
        xa = V1_I - xf;
    elseif (HEL <= Z1_I) && (Z1_I <= ST)
        FP2 = [0 0.084e9 -2.8644e9-Z1_I];
        xf = roots(FP2);
        xa = V1_I - xf;
    elseif ST < Z1_I
        FP3 = [1.1697e4 0.036e9 0.93e9-Z1_I];
        xf2 = roots(FP3);
        xf = max(xf2(1), xf2(2));
        xa = V1_I - xf;
    end

%Implement solver
St0L = Z2_I; St0R = Z1_I;

%Fundemental Interaction Solving Equations
F1 = [0 2*R_S*C_L -R_S*C_L*(xa+xb)];
F2 = [0 2*0.084e9 -0.084e9*(xa+xb)];
F3 = [0 2*R_S*(C_B+S*xb-S*xa) R_S*(S*(xa^2)-S*(xb^2)-C_B*(xa+xb))];
FT3 = [0 2*R_S*(C_B+S*xa-S*xb) R_S*(S*(xb^2)-S*(xa^2)-C_B*(xa+xb))];
```

```
%Find the correct interaction

% 1. Check for F1
x = roots(F1);
St = R_S*C_L*(x-xa);
if (0<=St) && (St<HEL) || (-HEL<=St) && (St<0)
    SW = St;
    u_p = x;
    if St <=0
        disp('Negative Stress 1');
    end
end

% 2. Check for F2
x = roots(F2);
St = 0.084e9*(x-xa)-2.8644e9;
if (HEL<=St) && (St<ST)
    SW = St;
    u_p = x;
    UR = C_B + S*(u_p - VI(1));
    UL = -C_B + S*(u_p - u_f);
end

% 3. Check for FT2
x = roots(F2);
St = 0.084e9*(x-xa)+2.8644e9;
if (-ST<=St) && (St<-HEL)
    disp('Negative Stress 2');
    SW = St;
    u_p = x;
    UR = C_B + S*(u_p - VI(1));
    UL = -C_B + S*(u_p - u_f);
end

% 4. Check for F3
x = roots(F3);
St = R_S*C_B*(x-xa)+R_S*S*(x-xa)^2+0.93e9;
if (ST<=St)
    SW = St;
    u_p = x;
    UR = C_B + S*(u_p - VI(1));
    UL = -C_B + S*(u_p - u_f);
end

%5. Check fot FT3
x = roots(FT3);
St = R_S*C_B*(x-xa)-R_S*S*(x-xa)^2-0.93e9;
if (St<-ST)
    disp('Negative Stress 3');
    SW = St;
    u_p = x;
    UR = C_B + S*(u_p - VI(1));
    UL = -C_B + S*(u_p - u_f);
end

%Check the seperation
if SW<=0
    f=1;
end

%Forward wave in target
if (St0R< HEL && SW > HEL) || (St0R> HEL && SW < HEL)


    %Foregoing Shock Wave
    active = [active,SW];
    c = [c,UR];
    v = [v,u_p];
```

```
    x0 = [x0,D1_I];
    t0 = [t0,t0_I+t1_I];
    stf = [stf, St0R];

elseif (St0R>= HEL && SW >= HEL)
   %Foregoing Shock Wave
    active = [active,SW];
    c = [c,UR];
    v = [v,u_p];
    x0 = [x0,D1_I];
    t0 = [t0,t0_I+t1_I];
    stf = [stf, St0R];

elseif (St0R< HEL && SW < HEL)
   %Foregoing elastic Wave
   if abs(SW-St0R)>= 1e-9*HEL
       active = [active,SW];
       c = [c,C_L];
       v = [v,u_p];
       x0 = [x0,D1_I];
       t0 = [t0,t0_I+t1_I];
       stf = [stf, St0R];
   end
end

%update the material interface stress and velocity
SI(1) = SW;
VI(1) = u_p;

%Backward wave in target
if (St0L< HEL && SW > HEL) || (St0L> HEL && SW < HEL)


    %Foregoing Shock Wave
    active = [active,SW];
    c = [c,UL];
    v = [v,u_p];
    x0 = [x0,D1_I];
    t0 = [t0,t0_I+t1_I];
    stf = [stf, St0L];

elseif (St0L>= HEL && SW >= HEL)
   %Foregoing Shock Wave
    active = [active,SW];
    c = [c,UL];
    v = [v,u_p];
    x0 = [x0,D1_I];
    t0 = [t0,t0_I+t1_I];
    stf = [stf, St0L];

elseif (St0L< HEL && SW < HEL)
   %Foregoing elastic Wave
   if abs(SW-St0L)>= 1e-9*HEL
       active = [active,SW];
       c = [c,-C_L];
       v = [v,u_p];
       x0 = [x0,D1_I];
       t0 = [t0,t0_I+t1_I];
       stf = [stf, St0L];
   end
end

    %Stress History, Velocity History Profiles
    if D0_I <= P && P <= 0
        t_p = t0_I + (P-D0_I)/C(I);
        Z_P = [Z_P, Z2_I]; T_P = [T_P,t_p]; V_P = [V_P, V2_I];
    end
```